**Table 1. A List of Identified Proteins**

| Accession No.* | Identified Protein* | Locus† | Spot No.† | *P* Value* | pI (cal)‖ | MW (cal) (D)‖ | Protein Score¶ | Peptide Matches | Sequence Coverage (%) |
|---|---|---|---|---|---|---|---|---|---|
| Proteins in cluster A** | | | | | | | | | |
| Function | | | | | | | | | |
| Cell proliferation | | | | | | | | | |
| P12004 | Proliferating cell nuclear antigen | 20pter-p12 | 2794 | 1.93E-03 | 4.57 | 29092 | 94 | 2 | 10 |
| | | | 2800 | 4.65E-03 | 4.57 | 29092 | 189 | 2 | 10 |
| | | | 2892 | 3.04E-03 | 4.57 | 29092 | 245 | 4 | 16.1 |
| Q15691 | APC-binding protein EB1 | 20q11.1-q11.23 | 3360 | 7.64E-03 | 5.02 | 30020 | 189 | 4 | 20.6 |
| P51858 | Hepatoma-derived growth factor | 1q21-q23 | 2938 | 4.54E-03 | 4.7 | 26886 | 200 | 4 | 21.7 |
| Protein folding | | | | | | | | | |
| P14625 | Heat shock protein 90 kDa beta member 1 | 12q24.2-q24.3 | 1696 | 2.89E-03 | 4.76 | 92696 | 267 | 5 | 6.5 |
| | | | 1741 | 1.25E-03 | 4.76 | 92696 | 717 | 23 | 17.6 |
| Q9UHV9 | Prefoldin subunit 2 | 1q23.3 | 4730 | 5.86E-03 | 6.2 | 16695 | 186 | 3 | 22.7 |
| Cytoskeletal/structural protein | | | | | | | | | |
| P20700 | Lamin-B1 | 5q23.3-q31.1 | 1080 | 3.73E-03 | 5.11 | 66522 | 821 | 19 | 27.9 |
| P08670 | Vimentin | 10p13 | 1968 | 5.91E-03 | 5.06 | 53545 | 797 | 20 | 32.7 |
| Signal transduction | | | | | | | | | |
| P06702 | Protein S100-A9 | 1q21 | 4680 | 5.02E-03 | 5.71 | 13291 | 81 | 2 | 26.3 |
| Transport | | | | | | | | | |
| P61923 | Customer subunit zeta-1 | 12q13.2-q13.3 | 4530 | 8.44E-03 | 4.69 | 20242 | 117 | 2 | 11.9 |
| Proteins in cluster B** | | | | | | | | | |
| Amino acid metabolism | | | | | | | | | |
| O95954 | Formimidoyltransferase-cyclodeaminase | 21q22.3 | 1398 | 5.07E-03 | 5.58 | 59574 | 422 | 7 | 17.7 |
| | | | 1417 | 1.04E-03 | 5.58 | 59574 | 483 | 9 | 17.6 |
| | | | 1422 | 1.19E-03 | 5.58 | 59574 | 482 | 9 | 19.4 |
| Q00266 | S-pdenosylmethionine synthetase isoform type-1 | 10q22 | 2004 | 1.26E-03 | 5.86 | 44190 | 124 | 2 | 8.4 |
| P16930 | Fumarylacetoacetase | 15q23-q25 | 2110 | 2.62E-03 | 6.46 | 46743 | 214 | 4 | 9.3 |
| P05089 | Arginase-1 | 6q23 | 2630 | 1.67E-03 | 6.72 | 34884 | 274 | 6 | 17.7 |
| Q14749 | Glycine N-methyltransferase | 6p12 | 2696 | 7.85E-03 | 6.58 | 33046 | 158 | 3 | 14.3 |
| Oxidoreduction | | | | | | | | | |
| P32754 | 4-hydroxyphenylpyruvate dioxygenase | 12q24-qter | 2376 | 7.33E-03 | 6.5 | 44946 | 539 | 10 | 25.5 |
| | | | 2385 | 6.83E-03 | 6.5 | 44946 | 734 | 18 | 37 |
| NP_036335 | Glyoxylate reductase/hydroxypyruvate reductase | 9q12 | 2520 | 9.29E-03 | 7.01 | 36045 | 312 | 6 | 19.5 |
| | | | 2527 | 2.06E-03 | 7.01 | 36045 | 122 | 3 | 8.2 |
| O95154 | Aflatoxin B1 aldehyde reductase member 3 | 1p35.1-p36.23 | 2884 | 5.26E-03 | 6.67 | 37582 | 412 | 6 | 23.6 |
| P78417 | Glutathione transferase omega-1 | 10q25.1 | 3824 | 2.73E-03 | 6.23 | 27833 | 202 | 4 | 18.3 |
| Lipid metabolism | | | | | | | | | |
| P54868 | Hydroxymethylglutaryl-CoA synthase, mitochondrial precursor | 1p13-p12 | 1709 | 1.60E-03 | 8.4 | 57113 | 174 | 3 | 6.5 |
| P45954 | Short/branched chain specific acyl-CoA dehydrogenase, mitochondrial precursor | 10q26.13 | 2428 | 8.62E-03 | 6.53 | 47797 | 469 | 8 | 21.8 |
| P16219 | Short-chain specific acyl-CoA dehydrogenase, mitochondrial precursor | 12q22-qter | 2526 | 1.01E-03 | 8.13 | 44611 | 683 | 16 | 35.7 |
| | | | 2542 | 2.69E-03 | 8.13 | 44611 | 376 | 8 | 17.7 |
| P30084 | Enoyl-CoA hydratase, mitochondrial precursor | 10q26.2-q26.3 | 3294 | 7.45E-03 | 8.34 | 31823 | 242 | 3 | 16.9 |

**Table 1. (Continued)**

| Accession No.* | Identified Protein* | Locus† | Spot No.† | *P* Value* | pI (cal)‖ | MW (cal) (D)‖ | Protein Score¶ | Peptide Matches | Sequence Coverage (%) |
|---|---|---|---|---|---|---|---|---|---|
| | | | 3304 | 8.65E-03 | 8.34 | 31823 | 116 | 2 | 9.7 |
| | | | 3332 | 8.74E-03 | 8.34 | 31823 | 205 | 6 | 16.9 |
| | | | 3338 | 8.69E-03 | 8.34 | 31823 | 529 | 12 | 31.7 |
| | | | 3378 | 8.67E-03 | 8.34 | 31823 | 287 | 5 | 20 |
| | | | 3402 | 6.06E-03 | 8.34 | 31823 | 308 | 5 | 22.8 |
| | | | 3420 | 4.11E-03 | 8.34 | 31823 | 290 | 8 | 20 |
| | | | 3465 | 4.17E-03 | 8.34 | 31823 | 473 | 8 | 31.4 |
| Chycometabolism | | | | | | | | | |
| P05062 | Fructose-bisphosphate aldolase B | 9q21.3-q22.2 | 2187 | 5.79E-03 | 8 | 39961 | 195 | 3 | 9.6 |
| P09467 | Fructose-1,6-bisphosphatase 1 | 9q22.3 | 2661 | 8.97E-03 | 6.6 | 37059 | 486 | 11 | 36.5 |
| Signal transduction | | | | | | | | | |
| P52566 | Rho GDP-dissociation Inhibitor 2 | 12p12.3 | 4046 | 1.49E-03 | 5.1 | 22900 | 136 | 2 | 15 |
| Isomerization | | | | | | | | | |
| P30039 | MAWD-binding protein | 10pter-q25.3 | 3284 | 5.68E-03 | 6.06 | 32050 | 118 | 2 | 8.7 |

*Proteins in Supporting Fig. 3 are shown as bold.

*Accession numbers of proteins and protein name were derived from Swiss-Prot and NCBI nonredundant databases.

Protein function was categorized by accessing Gene Ontology database (http://www.geneontology.org/) and literature curation.

†Gene locus was determined according to NCBI database.

‡Spot numbers refer to those in Figure 2C and Supplemental Fig. 1.

§Bonferroni adjusted *P* value.

‖Theoretical isoelectric point and molecular weight obtained from Swiss-Prot and the ExPASy database (http://au.expasy.org).

¶Mascot score for the identified proteins based on the peptide ions score ($P < 0.05$) (http://www.matrixscience.com).

**Cluster A and B are shown in Fig. 2C.

presently remains dismal, and novel diagnostic and therapeutic modalities, or improvement of existing therapeutic strategies, have long been required to improve the clinical outcome of patients with HCC.

Histological differentiation is a hallmark of malignant potential of HCC; patients with poorly-differentiated tumors tend to have worse prognosis than those with well-differentiated tumors.[6] Therefore, the molecular background of histological differentiation may involve prognostic biomarker candidates, which may lead to novel diagnostic and therapeutic modalities. However, although several factors regulating histological differentiation have been reported,[7,8] proteins that underlie HCC differentiation and correlate with HCC prognosis are presently unclear.

Recently, the advent of novel technologies linked with the Human Genome Database enabled global protein expression studies, namely proteomics.[9] The proteome is the functional translation of the genome, directly regulating cancer behavior, and is thus a rich source for identifying biomarkers and therapeutic targets. Proteomic studies have identified the proteins whose expression correlates with early recurrence of HCC.[10,11] The proteins implicated in early recurrence may have a clinical utility in predicting poor prognosis. Recently, we identified the proteins associated with histological differentiation in esophageal cancer using two-dimensional difference gel electrophoresis (2D-DIGE).[12] As the identified proteins included those associated with malignant attributes of tumor cells such as lymph node metastasis, this approach is also worth being applied to the study of HCC.

We conducted a proteomic study on HCC tissues with varying degrees of histological differentiation, as well as adjacent nontumor tissues and normal liver tissues, and captured a molecular signature that underlies HCC differentiation and affects the malignant potential of HCC. We found that expression of APC-binding protein EB1 (EB1) was specific to moderately-differentiated and poorly-differentiated HCCs, and revealed the prognostic value of EB1 expression, employing immunohistochemistry on additional HCC cases.

## Materials and Methods

Detailed procedures are available in the Supporting Information.

***Patients and Tissue Samples.*** A total of 45 surgically resected tissues were included in this study. The tissue samples were divided into five groups according to their histological classification: seven normal liver tissues, 11 nontumor tissues adjacent to tumors, six well-differentiated HCCs, 14 moderately-differentiated HCCs, and seven poorly-differentiated HCCs (Supporting Table 1). The tissues were obtained at the National Cancer Center Hospital; the HCC and adjacent nontumor tissues were from patients with HCC who underwent initial hepatic resection between June 2005 and April 2006, and the normal liver tissues were from patients who underwent hepatic resection for metastatic liver tumor from colorectal cancer in the same period. Different histological areas of HCC were obtained from identical tumor tissues of three cases whose tumors showed histological heterogeneity. The clinicopathological features of the patients are listed in Supporting Table 1. For the EB1 expression study, we examined an additional 145 patients with HCC who underwent initial surgical resection between February 1992 and December 2000 at the National Cancer Center Hospital. None of the patients of this study received any preoperative therapy. Tumors were classified according to the World Health Organization classification[13] and the International Union against Cancer tumor-node-metastasis (TNM) classification.[14] The ethical review board of the National Cancer Center approved this project.

***Laser Microdissection.*** Specific populations of cells were recovered by laser microdissection according to our previous reports[15,16] (Fig. 1A). In brief, 10-$\mu$m-thick frozen sections were created from tumor tissues and stained with hematoxylin. The cells were recovered under microscopic observation with the assistance of a ultraviolet laser (MMI CellCut; Molecular Machines & Industries, Glattbrugg, Switzerland). A 1-mm$^2$ tissue area (~3,000 cells) was recovered for one gel. The recovered cells were lysed in urea lysis buffer containing 6 M urea, 2 M thiourea, 3% {3-[(3-cholamidopropyl)dimethylammonio]-1-propanesulfonate}, and 1% Triton X-100, and were stored at −80°C until use.

***2D-DIGE and Image Analysis.*** The 2D-DIGE was performed as described.[15,16] In brief, a common internal control sample was created by mixing a small portion of all protein samples used in this study, and labeled with cyanine 3 (Cy3) fluorescent dye (CyDye DIGE Fluor saturation dye; GE Healthcare Biosciences, Uppsala, Sweden). Individual samples were labeled with cyanine 5 (Cy5) fluorescent dye (CyDye DIGE Fluor saturation dye; GE Healthcare Biosciences). These differently-labeled protein samples were mixed together and separated according to their isoelectric point and molecular weight. The first dimension separation was achieved using a 24-cm-length immobiline gel (IPG, pI 4-7; GE Healthcare Biosciences) and Multiphor II (GE Healthcare Biosciences), while the second-dimension separation used a homemade gradient gel with GiantGelRunner (Biocraft, Tokyo, Japan), with a separation distance of 36 cm. The gels were scanned using a laser scanner (Typhoon Trio; GE Healthcare Biosciences) at the appropriate wavelength for Cy3 or Cy5. For all protein spots, the Cy5

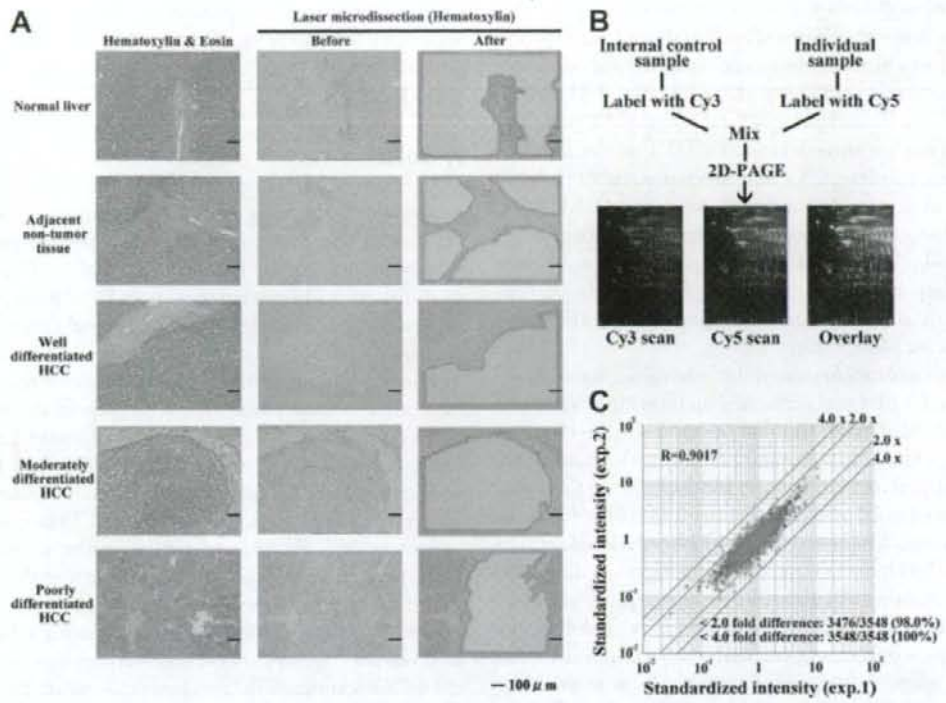


Fig. 1. Protein expression profiling using laser microdissection and 2D-DIGE with high sensitive fluorescent dyes. (A) Specific populations of cells were recovered using laser under microscopic observation. (B) The extracted proteins were labeled with fluorescent dyes and separated by two-dimensional polyacrylamide gel electrophoresis (2D-PAGE). (C) Evaluation of the reproducibility of 2D-DIGE by scatter graphs.

intensity was normalized with the Cy3 intensity in the same gel using the DeCyder software (version 5.0; GE Healthcare Biosciences), so that gel-to-gel variations were canceled out (Fig. 1B). We monitored the reproducibility of our system by running the same sample twice (case 24; Supporting Table 1). The scatter-plot demonstrated that the intensity value of 98% of protein spots was scattered within a two-fold difference, and that the correlation coefficient was 0.9017, showing the high reproducibility of the profiling method used (Fig. 1C). The spot intensity data were exported from the DeCyder software as extensible markup language (XML) format files, which are amenable to data analysis.

***Data Analysis.*** The numerical data in the XML files were imported to Expressionist software (GeneData, Basel, Switzerland) for scatter-plotting, hierarchical clustering, and principal component analysis. The Kruskal-Wallis test and Bonferroni adjustment were used to identify the protein spots that were differentially expressed in the five tissue groups examined.

***Mass Spectrometric Protein Identification.*** The proteins corresponding to the protein spots were identified by mass spectrometry according to our report.[12] Cy5-labeled proteins separated by 2D-polyacrylamide gel electrophoresis (PAGE) were recovered in gel plugs and digested with modified trypsin (Promega, Madison, WI). The trypsin digests were subjected to liquid chromatography, coupled with tandem mass spectrometry equipped with a nanoelectrospray ion source (Paradigm MS4 dual solvent delivery system; Michrom BioResources Inc., Auburn, CA) for microflow high-performance liquid chromatography (HPLC), an HTS PAL auto sampler (CTC Analytics, Zwingen, Switzerland), and a Finnigan LTQ linear ion trap mass spectrometer (ThermoElectron Co., San Jose, CA) equipped with a nanoelectrospray ion source (AMR Inc., Tokyo, Japan). The Mascot software (version 2.1; Matrix Science, London, UK) was used to search for the mass of the peptide ion peaks against the SWISS-PROT database (*Homo sapiens*; 12867 sequence in Sprot_47.8 fasta file). Proteins with a Mascot score of 35 or more were used for protein identification. When multiple proteins were identified in a single spot, the proteins with the highest number of peptides were considered as those corresponding to the spot.

***Western Blotting.*** Protein samples were separated by sodium dodecyl sulfate (SDS)-PAGE and subsequently blotted on a nitrocellulose membrane. Immunoblot analysis was performed using the antibodies EB1 (1:200; Santa Cruz Biotechnology, Santa Cruz, CA), proliferating cell nuclear antigen (1:5,000; BD Transduction Laboratories, San Jose, CA), heat shock protein 90 (1;1,000; BD Transduction Laboratories), arginase-I (1;1,000; BD Transduction Laboratories), actin (1;2;000; Abcam, Cambridge, UK), horseradish peroxidase–conjugated secondary antibodies (1:1,000; GE Healthcare Biosciences), and enhanced chemiluminescence (ECL; GE Healthcare Biosciences).

***Immunohistochemistry.*** Immunohistochemical staining for EB1 was performed on formalin-fixed, paraffin-embedded tissue sections using the CSA II system (DAKO, Glostrup, Denmark) following the manufacturer's instructions. For antigen retrieval, the sections were autoclaved in 10 mM citrate buffer (pH 6.0) at 121°C for 10 minutes. We used rabbit anti-EB1 polyclonal antibodies (sc-15347; Santa Cruz Biotechnology) at a dilution of 1:500. Staining was assessed by two independent observers in a blinded fashion for clinical data. The bile duct epithelium served as an internal control of positive staining. If more than 50% of tumor cells were positively stained, the tumor was judged as EB1-positive. Staining evaluation was done at the dominant differentiation area of the tumor if the tumor had areas with varying degrees of differentiation.

***Pathway Analysis of Expression Data.*** The pathway analysis of the protein expression pattern was performed using the MetaCore software (GeneGo Inc., St. Joseph, MI). MetaCore identifies networks based on a manually curated database containing known molecular interactions, functions, and disease interrelationships, using proteome data sets. The pathways were identified by the probability that a random set of proteins the same size as the input list would give rise to a particular mapping by chance.

***Statistical Analysis.*** The correlation between EB1 expression and clinicopathological features was evaluated by the Fisher exact test for categorical variables and the Mann-Whitney *U* test for continuous variables. The time to recurrence and overall survival were calculated from the first resection of the primary tumor to the first radiological evidence of recurrence or to death, respectively. All time-to-event end points were computed by the Kaplan-Meier method.[17] Patients dying without recurrence were censored in determining recurrence. Potential prognostic factors were identified by univariate analysis using the log-rank test. Independent prognostic factors were evaluated using a Cox proportional hazards regression model and a stepwise selection procedure. *P* differences $<0.05$ were considered to be significant. Statistical analyses were performed using the SPSS statistical package (SPSS, Chicago, IL).

## Results

***Proteomic Profiling of HCC.*** To examine the overall features of the proteome, we performed unsupervised classification using the intensity values of 3,319 protein spots that were observed in more than 80% of the protein expression profiles of the common internal control sample. Results of hierarchical clustering were associated with histological grouping: the seven normal liver tissues, 11 adjacent nontumor tissues, six well-differentiated HCCs, and one moderately-differentiated HCC were grouped together, while the 13 moderately-differentiated HCCs and seven poorly-differentiated HCCs were clustered together forming a separate group (Fig. 2A). Principal component analysis also showed similar results; normal and adjacent nontumor tissues were grouped together while well-differentiated tumors were segregated from the group of moderately-differentiated or poorly-differentiated tumors (Fig. 2B). These observations suggested that the overall features of the proteome may reflect the major histological patterns.

To identify the proteins that are differentially expressed in the five tissue groups examined, we performed a Kruskal-Wallis test and applied Bonferroni adjustment. We selected the protein spots such that the Bonferroni adjusted *P* value was $<0.01$ and the expression ratio between groups with the greatest difference was at least three times or more. Consequently, we found 41 protein spots meeting this criterion (Supporting Fig. 1). The expression pattern of these selected 41 protein spots in all tissue samples is shown in Fig. 2C. Using hierarchical clustering, we found that the protein spots were subdivided into clusters A and B, based on whether their intensity was upregulated or downregulated in the group of moderately-differentiated HCCs and poorly-differentiated HCCs (Fig. 2C).

***Protein Identification and Network Analysis.*** Mass spectrometric study resulted in the identification of 26 unique proteins corresponding to the 41 protein spots (Fig. 2C, right side; Table 1; Supporting Table 2). Functional classification according to Gene Ontology (www.geneontology.org) demonstrated that a large proportion of the identified proteins are involved in amino acid metabolism, oxidoreduction, and lipid metabolism (Fig. 3A; Table 1). The proteins corresponding to the protein spots in clusters A and B were classified according to their known function (Fig. 3B,C; Table 1). Proteins in clusters

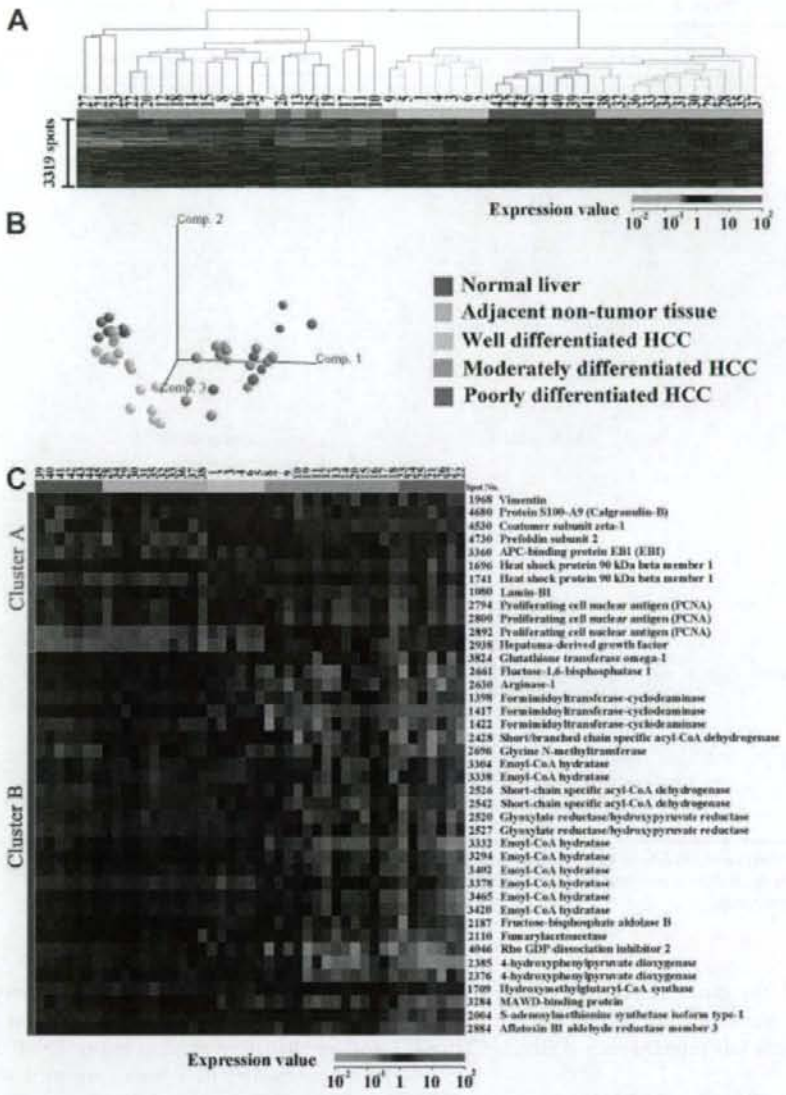


Fig. 2. Proteomic classification of tissue samples and identification of proteins with different expression levels between the sample groups. (A) Hierarchical clustering and (B) principal component analysis grouped the tissue samples based on the intensity of 3319 protein spots. (C) Heat map of the 41 selected protein spots is shown. The results of protein identification are demonstrated in the right side of (C).

A included ones involved in cell proliferation, protein folding, and cytoskeletal/structural proteins. Proteins in cluster B included ones involved in amino acid metabolism, oxidoreduction, and lipid metabolism, all of which maintain normal hepatic functions. Western blotting results were consistent with the 2D-DIGE results, validating the differential expression of the identified proteins (Supporting Fig. 2A,B).

We explored the biological significance of the altered protein expression patterns by classifying the associated proteins within the context of functional pathways and networks using MetaCore, and we found that 14 of the 26 identified proteins could be functionally linked (Supporting Fig. 3). The transcription factors in this network included c-Myc, hepatocyte nuclear factor 4 alpha, AP-1, HIF1A, and C/EBP beta, which connected five, five,

**Table 2. Correlations Between Clinicopathological Features and EB1 Expression**

| Variable | EB1 Positive (Number of Cases) | EB1 Negative (Number of Cases) | Correlation (EB1) *P* Value* |
|---|---|---|---|
| Age† | 61 (48-80) | 65 (26-83) | 0.161 |
| Gender | | | 0.825 |
| Female | 8 | 25 | |
| Male | 32 | 80 | |
| Virus infection status | | | 0.302 |
| HBV | 15 | 31 | |
| HCV | 17 | 60 | |
| Both | 5 | 6 | |
| None | 3 | 8 | |
| Child-Pugh Classification | | | 1.000 |
| A | 37 | 97 | |
| B | 3 | 8 | |
| Liver cirrhosis | | | 0.502 |
| Absence | 32 | 77 | |
| Presence | 8 | 28 | |
| AFP (ng/mL)† | | | **<0.001** |
| | 343.5 (3-27170) | 20.3 (1-9994) | |
| TNM Stage | | | **<0.001** |
| I or II | 20 | 89 | |
| III or IV | 20 | 16 | |
| Tumor number | | | 1.000 |
| Single | 31 | 81 | |
| Multiple | 9 | 24 | |
| Tumor size (mm)† | | | **0.008** |
| | 45 (13-155) | 30 (6-185) | |
| Differentiation | | | **<0.001** |
| Well differentiated | 0 | 24 | |
| Moderately differentiated | 9 | 73 | |
| Poorly differentiated | 31 | 8 | |
| Portal vein invasion | | | **<0.001** |
| Absence | 8 | 79 | |
| Presence | 32 | 26 | |
| Intrahepatic metastasis | | | **<0.001** |
| Absence | 22 | 90 | |
| Presence | 18 | 15 | |

Bold indicates significant values. HBV, hepatitis B virus; HCV, hepatitis C virus; AFP, alpha-fetoprotein
*Fisher exact test for categorical variables and Mann-Whitney *U* test for continuous variables.
†Expressed as median (range).

three, two, and one genes, respectively. Other proteins responsible for the regulation of multiple proteins included Ras superfamily proteins such as RhoA, CDC42, and Rac1.

***Clinical Significances of EB1 Expression in HCC.*** Among the identified proteins, EB1 is controlled by c-Myc, RhoA and CDC42, which have all been linked to HCC malignancy in previous reports[18-21] (Fig. 3D). For this reason, we further examined the relationship of EB1 with certain clinicopathological parameters in an additional 145 HCC cases that were not included in the proteomic study, employing immunohistochemistry. Immunohistochemical staining for EB1 was observed in the cytoplasm of tumor cells, inflammatory cells, and bile duct epithelium, while hepatocytes in nontumor areas showed no immunostaining (Fig. 4). The EB1-positive and EB1-negative tumor tissues had significantly different histological differentiation, alpha-fetoprotein expression, TNM stage, tumor size, portal vein invasion status, and intrahepatic metastasis status ($P < 0.01$; Table 2). As these parameters have been correlated with the clinical outcome of patients with HCC, we further investigated the correlation of EB1 with prognostic data. As shown in the Kaplan-Meier survival curve (Fig. 5), patients with EB1-positive HCC tumors had significantly worse prognosis than those with EB1-negative HCC tumors, in terms of both overall survival rate ($P < 0.0001$) and cumulative recurrence rate ($P < 0.0001$). Univariate and multivariate analyses revealed that EB1 is an independent prognostic factor for overall survival (hazard ratio, 2.256; 95% confidence interval, 1.337-3.807; $P = 0.002$) and recurrence (hazard ratio, 2.740; 95% confidence interval, 1.771-4.239; $P < 0.001$) along with other established clinicopathological parameters such as liver cirrhosis, por-

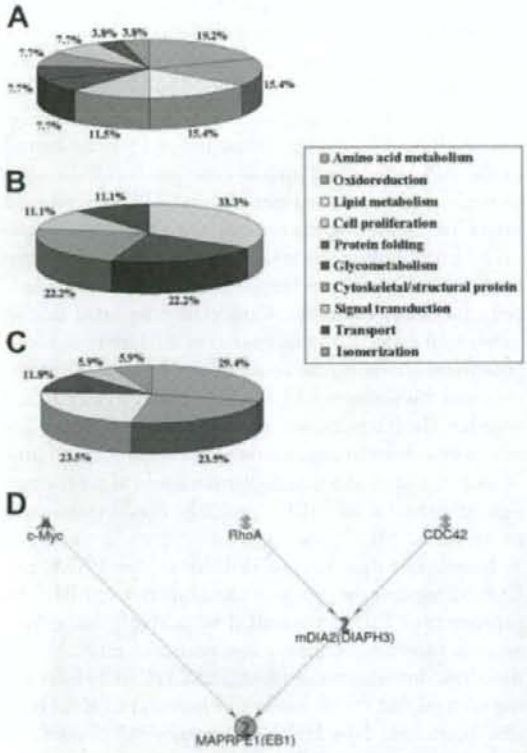


Fig. 3. Functional classification and network analysis of the identified proteins. (A) Functional classification of all proteins, (B) proteins in cluster (A), and (C) proteins in cluster (B). Clusters (A) and (B) are shown in Fig. 2. (D) EB1 is controlled by c-Myc, RhoA, and CDC42, which have all been linked to HCC malignancy. The differently colored nodes represent transcription factors (red shape), Ras-superfamilies (light blue shapes), and other proteins (blue shapes). The green line indicates a positive effect and the gray indicates an unspecified effect.

tal vein invasion, tumor number, and intrahepatic metastasis (Table 3).

## Discussion

The need for improvement of the management of HCC has led to a strong demand for the development of novel prognostic biomarkers for HCC. Global genomic and transcriptomic expression studies have been conducted to detect such prognostic molecular biomarkers for HCC. For example, using array-based comparative genomic hybridization analysis, chromosomal loss on 17p13.3 and gain on 8q11 were shown to have significant effects on patient outcome.[22] Using complementary DNA microarray technology, osteopontin was identified as a critical player in HCC metastasis,[23] and AP-1 transcription factors were shown to have key roles in the development of a poor-prognosis subtype of HCC.[24] In contrast, few such studies have been performed using a proteomic approach.[11] Here we present the results of such a proteomic study, and propose EB1 as a prognostic biomarker for HCC.

In this study, we examined HCC tissues classified according to their histological differentiation. As the degree of histological differentiation is a hallmark of the malignant potential of HCC, the proteomic background of HCC differentiation may involve key proteins for HCC progression. Unsupervised classification of tissues based on their protein expression profiles without any *a priori* assumptions was associated with their histological presentation, indicating that the overall features of the proteome may reflect the major histological differences between tissues. We subsequently identified 26 proteins that showed the most variable expression between the groups with different histology.

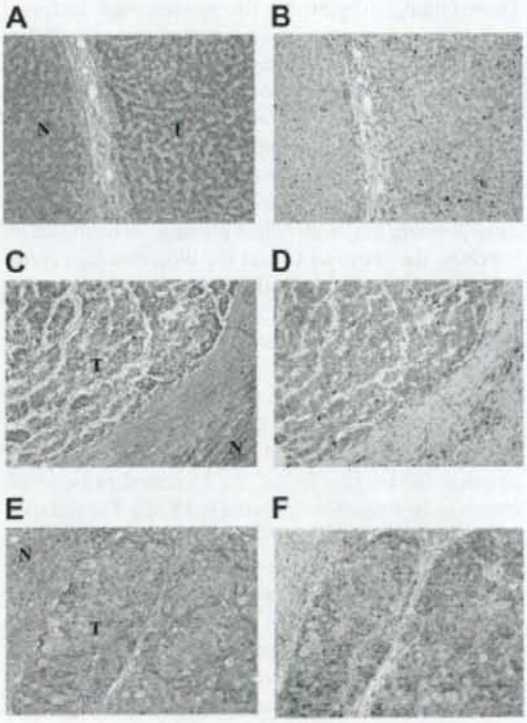


Fig. 4. Expression of EB1 in HCC tissues with different histological differentiation. (A,B) Well-differentiated, (C,D) moderately-differentiated, (E,F) and poorly-differentiated HCCs were examined. (A,C,E) Hematoxylin and eosin-stained tissues; (B,D,F) tissues stained with anti-EB1 antibody. Note that EB1 expression correlated with the degree of histological differentiation. Nontumor liver and HCC are indicated by (N) and (T), respectively.

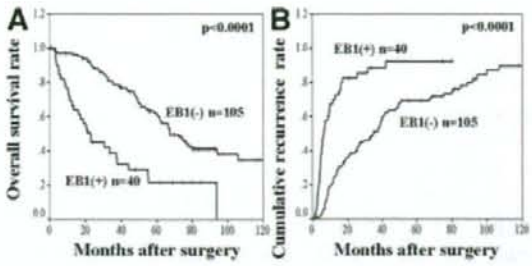


Fig. 5. Correlation of EB1 expression with clinical outcome of HCC patients after curative resection. The patients with HCC tissues showing EB1 expression had poorer prognosis in terms of (A) overall survival and (B) overall recurrence.

Functional classification demonstrated that proteins associated with cell proliferation, protein folding, and cytoskeletal structure were increased, and proteins associated with amino acid metabolism, oxidoreduction, and lipid metabolism were reduced during HCC progression. These findings suggest that the proteins with increased expression during pathological progression have a different functional tendency compared to those with reduced expression. The different proteomic aberrations observed in the varying stages of cancer progression, as reflected in the different histology groups, are unlikely to represent random events. In contrast to the functional classification of the proteins, the chromosomal localization of the genes corresponding to the identified proteins, as identified by searching the National Center for Biotechnology Information database (Table 1), did not have an obvious tendency. These observations suggest that proteomic studies may provide unique information not generated by genomic studies.

Network analysis using literature mining revealed that the identified proteins were functionally linked to certain transcription factors and Ras superfamilies. The transcription factors that linked the identified proteins are known to be frequently activated in HCCs. For instance, c-Myc amplification has been frequently observed in HCCs and is associated with poor prognosis.[18,19] Liu et al.[25] have reported that AP-1 is frequently activated at the early stages of HCC. HIF1A is also important in the progression of hepatocarcinogenesis.[26] Other proteins responsible for the regulation of multiple proteins have also been reported to be correlated with HCC malignancy. Overexpression of RhoA[20] is associated with poor prognosis in HCC, and Rac activation is associated with metastasis of HCC.[27] Activation of CDC42 was involved in the metastasis of HCC cells.[21] The proteins we identified may be downstream effectors of known key regulators of carcinogenesis and tumor progression. Although correlations between these molecules and HCC progression have been independently and separately reported, the present global protein expression study enabled a panoramic view of the molecular background of the progression of HCC.

Our study showed the prognostic value of EB1 expression in HCC. EB1 has been identified as a protein bound to the APC tumor suppressor gene product.[28] In vitro wounding assays revealed that EB1 and APC promote cell migration, stabilizing microtubules in a coordinate manner.[29] EB1 inhibits the ability of APC to bind to actin filaments, which may be required for maintenance of cell-cell adhesion.[30] Recently, Wang et al.[31] reported that in esophageal cancer, overexpression of EB1 promotes cell growth by activating the beta-catenin/T-cell factor pathway, and this pathway is often activated in HCC.[32] Taken together, the interaction of EB1 and APC may play a key role in cytoskeleton organization, cell migration and proliferation, and its aberrant regulation could affect the malignant behavior of HCC, probably resulting in poor prognosis for HCC patients.

Network analysis has revealed that c-Myc, RhoA, and CDC42 regulate the expression and function of EB1. The expression of EB1 is controlled by c-Myc[33] and c-Myc amplification has prognostic significance in HCC.[18] EB1 functions downstream of RhoA and CDC42 by interacting with mDia2,[29,34,35] and both RhoA and CDC42 have also been linked to HCC malignancy.[20,21] Taken together, we considered that EB1 may also be associated with poor prognosis.

Our findings can be of use in the search for biomarker identification and development. We studied the relationship of EB1 expression with clinical outcome of the HCC patients in additional 145 cases. Univariate and multivariate analyses revealed that EB1 is an independent prognostic factor for both recurrence and survival of HCC patients. Our results indicate that EB1 expression may be used as a novel prognostic biomarker of HCC. The correlation between EB1 expression and prognosis in HCC has not been examined or demonstrated previously.

The expression of EB1 was observed only in moderately or poorly differentiated HCC in this study (Table 2), and the prognostic utility of EB1 expression is therefore limited to patients with these tumors. The overall survival rate of patients with well-differentiated HCC was significantly higher than that of patients with poorly-differentiated or moderately-differentiated tumors (Table 3), a finding that is consistent with the report by Ariizumi et al.,[36] in which the 5-year survival rate was 78.1%, 49.0%, and 37.4% for the well-differentiated, moderately-differentiated, and poorly-differentiated tumors, respectively. The evaluation of EB1 expression could therefore provide prognostic information for the sub-

**Table 3. Univariate and Multivariate Analyses of Prognostic Factors for Patients with HCC**

| | | Univariate Analysis | | | |
|---|---|---|---|---|---|
| | | Survival | | Recurrence | |
| Variable | n | 5-Years (%) | *P* Value | 5-Years (%) | *P* Value |
| Age* | | | **0.7909** | | 0.6517 |
| <64 | 76 | 53.8 ± 6.2 | | 77.8 ± 5.2 | |
| ≥64 | 69 | 48.8 ± 6.3 | | 73.7 ± 5.5 | |
| Gender | | | 0.9721 | | 0.9862 |
| Female | 33 | 51.6 ± 9.2 | | 78.1 ± 7.5 | |
| Male | 112 | 51.3 ± 5.1 | | 75.2 ± 4.4 | |
| Virus infection status | | | **0.3794** | | 0.0827 |
| HBV | 46 | 53.1 ± 8.0 | | 60.0 ± 7.8 | |
| HCV | 77 | 54.3 ± 6.1 | | 81.1 ± 4.6 | |
| Both | 11 | 36.4 ± 14.5 | | 87.9 ± 11.0 | |
| None | 11 | 40.0 ± 15.5 | | 81.8 ± 11.6 | |
| Child-Pugh Classification | | | **0.0407** | | 0.1315 |
| A | 134 | 52.9 ± 4.6 | | 74.7 ± 4.0 | |
| B | 11 | 34.1 ± 15.0 | | 100.0 ± 0.0 | |
| Liver cirrhosis | | | **0.0277** | | 0.6586 |
| Absence | 109 | 57.6 ± 5.1 | | 74.6 ± 4.4 | |
| Presence | 36 | 35.2 ± 8.1 | | 79.0 ± 7.4 | |
| AFP* | | | **0.0532** | | **0.0210** |
| <27.2 | 70 | 60.4 ± 6.2 | | 67.1 ± 6.1 | |
| ≥27.2 | 73 | 41.4 ± 6.2 | | 85.8 ± 4.3 | |
| TNM Stage | | | **<0.0001** | | **<0.0001** |
| I or II | 109 | 61.9 ± 5.0 | | 69.6 ± 4.7 | |
| III or IV | 36 | 16.2 ± 7.1 | | 94.3 ± 3.9 | |
| Tumor number | | | 0.0856 | | **0.0238** |
| Single | 112 | 55.9 ± 5.0 | | 70.9 ± 4.6 | |
| Multiple | 33 | 36.8 ± 9.0 | | 90.9 ± 5.0 | |
| Tumor size (mm)* | | | 0.0627 | | **0.0178** |
| <35 | 66 | 62.1 ± 6.3 | | 72.9 ± 5.8 | |
| ≥35 | 79 | 42.5 ± 6.0 | | 78.2 ± 4.9 | |
| Differentiation | | | **<0.0001** | | **<0.0001** |
| Well differentiated | 24 | 73.9 ± 9.2 | | 76.3 ± 9.2 | |
| Moderately differentiated | 82 | 59.6 ± 5.8 | | 66.2 ± 5.6 | |
| Poorly differentiated | 39 | 16.3 ± 7.3 | | 95.9 ± 3.8 | |
| Portal vein invasion | | | **<0.0001** | | **0.0001** |
| Absence | 87 | 67.7 ± 5.3 | | 68.4 ± 5.3 | |
| Presence | 58 | 24.7 ± 6.4 | | 86.6 ± 4.8 | |
| Intrahepatic metastasis | | | **<0.0001** | | **<0.0001** |
| Absence | 112 | 60.7 ± 4.9 | | 70.6 ± 4.6 | |
| Presence | 33 | 19.0 ± 7.4 | | 93.7 ± 4.3 | |
| EB1 expression | | | **<0.0001** | | **<0.0001** |
| Negative | 105 | 62.1 ± 5.0 | | 69.3 ± 4.8 | |
| Positive | 40 | 22.0 ± 7.4 | | 92.2 ± 4.7 | |

| | Multivariate Analysis | | | | |
|---|---|---|---|---|---|
| | Beta | SE | HR | 95% CI | *P* value |
| Survival | | | | | |
| Liver cirrhosis | 0.922 | 0.258 | 2.515 | 1.517-4.170 | **<0.001** |
| Portal vein invasion | 0.670 | 0.301 | 1.955 | 1.083-3.528 | **0.026** |
| Intrahepatic metastasis | 0.699 | 0.289 | 2.012 | 1.143-3.544 | **0.015** |
| EB1 expression | 0.814 | 0.267 | 2.256 | 1.337-3.807 | **0.002** |
| Recurrence | | | | | |
| Tumor number | 0.594 | 0.213 | 1.811 | 1.192-2.752 | **0.005** |
| Intrahepatic metastasis | 1.030 | 0.227 | 2.802 | 1.795-4.375 | **<0.001** |
| EB1 expression | 1.008 | 0.223 | 2.740 | 1.771-4.239 | **<0.001** |

**Bold** indicates significant values. *Two groups were divided by the median. HBV, hepatitis B virus; HCV, hepatitis C virus; AFP, alpha-fetoprotein; Beta, regression coefficient; SE, standard error; HR, hazard ratio; CI, confidence interval.

groups of HCC, which could benefit from a more refined prognostic protocol.

Our list of identified proteins also included gene products reported as prognostic biomarker candidates (Fig. 2C). Expression of both hepatoma-derived growth factor[37] and proliferating cell nuclear antigen[38] have been correlated with poor differentiation, shorter survival periods, and higher incidence of recurrence in HCC patients. Overexpression of vimentin has been associated with the metastasis in HCC.[39] The relation between HCC differentiation and poor prognosis may be explained by these proteins and EB1, and the combined use of these biomarker candidates may improve the diagnosis and prognostic performance.

In conclusion, through the present global protein expression study the molecular background of histological differentiation in HCC was revealed and EB1 was established as a prognostic biomarker for both recurrence and survival. Poor outcomes in HCC are mainly due to postsurgical tumor recurrence, but recent advances in adjuvant therapies have improved survival periods for patients with recurrence.[40] The immunohistochemical examination of EB1 expression will help identify patients with high risk for recurrence, and close postoperative follow-up and additional treatment may improve the clinical outcome of these patients. Taken together, our results provide the possibility of novel strategies for HCC management.

*Acknowledgment:* The excellent technical support of Yukiko Fujie and Mina Fujishiro with the electrophoresis is greatly appreciated.

## References

1. Bosch FX, Ribes J, Borras J. Epidemiology of primary liver cancer. Semin Liver Dis 1999;19:271-285.
2. Pisani P, Parkin DM, Bray F, Ferlay J. Estimates of the worldwide mortality from 25 cancers in 1990. Int J Cancer 1999;83:18-29.
3. Parkin DM, Pisani P, Ferlay J. Estimates of the worldwide incidence of 25 major cancers in 1990. Int J Cancer 1999;80:827-841.
4. El-Serag HB, Mason AC. Rising incidence of hepatocellular carcinoma in the United States. N Engl J Med 1999;340:745-750.
5. Taylor-Robinson SD, Foster GR, Arora S, Hargreaves S, Thomas HC. Increase in primary liver cancer in the UK, 1979-94. Lancet 1997;350: 1142-1143.
6. Ker CG, Chen HY, Chen KS, Jeng IJ, Yang MY, Juan CC, et al. Clinical significance of cell differentiation in hepatocellular carcinoma. Hepatogastroenterology 2003;50:475-479.
7. Hu Z, Evarts RP, Fujio K, Marsden ER, Thorgeirsson SS. Expression of hepatocyte growth factor and c-met genes during hepatic differentiation and liver development in the rat. Am J Pathol 1993;142:1823-1830.
8. Suzuki T, Yano H, Nakashima Y, Nakashima O, Kojiro M. Beta-catenin expression in hepatocellular carcinoma: a possible participation of beta-catenin in the dedifferentiation process. J Gastroenterol Hepatol 2002;17: 994-1000.
9. Diamond DL, Proll SC, Jacobs JM, Chan EY, Camp DG 2nd, Smith RD, et al. HepatoProteomics: applying proteomic technologies to the study of liver function and disease. HEPATOLOGY 2006;44:299-308.
10. Yokoo H, Kondo T, Okano T, Nakanishi K, Sakamoto M, Kosuge T, et al. Protein expression associated with early intrahepatic recurrence of hepatocellular carcinoma after curative surgery. Cancer Sci 2007;98: 665-673.
11. Yi X, Luk JM, Lee NP, Peng J, Leng X, Guan XY, et al. Association of mortalin (HSPA9) with liver cancer metastasis and prediction for early tumor recurrence. Mol Cell Proteomics 2008;7:315-325.
12. Hatakeyama H, Kondo T, Fujii K, Nakanishi Y, Kato H, Fukuda S, et al. Protein clusters associated with carcinogenesis, histological differentiation and nodal metastasis in esophageal cancer. Proteomics 2006; 6:6300-6316.
13. Hirohashi S, Isak KG, Kojiro M, Wanless IR, Theise ND, Tsukuma H, et al. Hepatocellular carcinoma. Lyon, France: IARC Press; 2000:159-172.
14. Greene FL, Page DL, Fleming ID, Fritz A, Balch CM, Haller DG, et al. AJCC Cancer Staging Manual. 6th ed. Chicago: Springer; 2002:131-144.
15. Kondo T, Seike M, Mori Y, Fujii K, Yamada T, Hirohashi S. Application of sensitive fluorescent dyes in linkage of laser microdissection and two-dimensional gel electrophoresis as a cancer proteomic study tool. Proteomics 2003;3:1758-1766.
16. Kondo T, Hirohashi S. Application of highly sensitive fluorescent dyes (CyDye DIGE Fluor saturation dyes) to laser microdissection and two-dimensional difference gel electrophoresis (2D-DIGE) for cancer proteomics. Nat Protoc 2006;1:2940-2956.
17. Kaplan E, Meier P. Nonparametric estimation from incomplete observations. J Am Stat Assoc 1958;53:457-481.
18. Wang Y, Wu MC, Sham JS, Zhang W, Wu WQ, Guan XY. Prognostic significance of c-Myc and AIB1 amplification in hepatocellular carcinoma. A broad survey using high-throughput tissue microarray. Cancer 2002;95: 2346-2352.
19. Abou-Elella A, Gramlich T, Fritsch C, Gansler T. c-Myc amplification in hepatocellular carcinoma predicts unfavorable prognosis. Mod Pathol 1996;9:95-98.
20. Li XR, Ji F, Ouyang J, Wu W, Qian LY, Yang KY. Overexpression of RhoA is associated with poor prognosis in hepatocellular carcinoma. Eur J Surg Oncol 2006;32:1130-1134.
21. Xie L, Qin W, Li J, He X, Zhang H, Yao G, et al. BNIPL-2 promotes the invasion and metastasis of human hepatocellular carcinoma cells. Oncol Rep 2007;17:605-610.
22. Katoh H, Shibata T, Kokubu A, Ojima H, Loukopoulos P, Kanai Y, et al. Genetic profile of hepatocellular carcinoma revealed by array-based comparative genomic hybridization: identification of genetic indicators to predict patient outcome. J Hepatol 2005;43:863-874.
23. Ye QH, Qin LX, Forgues M, He P, Kim JW, Peng AC, et al. Predicting hepatitis B virus-positive metastatic hepatocellular carcinomas using gene expression profiling and supervised machine learning. Nat Med 2003;9: 416-423.
24. Lee JS, Heo J, Libbrecht L, Chu IS, Kaposi-Novak P, Calvisi DF, et al. A novel prognostic subtype of human hepatocellular carcinoma derived from hepatic progenitor cells. Nat Med 2006;12:410-416.
25. Liu P, Kimmoun E, Legrand A, Sauvanet A, Degott C, Lardeux B, et al. Activation of NF-kappa B, AP-1 and STAT transcription factors is a frequent and early event in human hepatocellular carcinoma. J Hepatol 2002;37:63-71.
26. Tanaka H, Yamamoto M, Hashimoto N, Miyakoshi M, Tamakawa S, Yoshie M, et al. Hypoxia-independent overexpression of hypoxia-inducible factor 1alpha as an early change in mouse hepatocarcinogenesis. Cancer Res 2006;66:11263-11270.
27. Lee TK, Poon RT, Yuen AP, Man K, Yang ZF, Guan XY, et al. Rac activation is associated with hepatocellular carcinoma metastasis by up-regulation of vascular endothelial growth factor expression. Clin Cancer Res 2006;12:5082-5089.
28. Su LK, Burrell M, Hill DE, Gyuris J, Brent R, Wiltshire R, et al. APC binds to the novel protein EB1. Cancer Res 1995;55:2972-2977.
29. Wen Y, Eng CH, Schmoranzer J, Cabrera-Poch N, Morris EJ, Chen M, et al. EB1 and APC bind to mDia to stabilize microtubules downstream of Rho and promote cell migration. Nat Cell Biol 2004;6:820-830.

30. Moseley JB, Bartolini F, Okada K, Wen Y, Gundersen GG, Goode BL. Regulated binding of adenomatous polyposis coli protein to actin. J Biol Chem 2007;282:12661-12668.
31. Wang Y, Zhou X, Zhu H, Liu S, Zhou C, Zhang G, et al. Overexpression of EB1 in human esophageal squamous cell carcinoma (ESCC) may promote cellular growth by activating beta-catenin/TCF pathway. Oncogene 2005;24:6637-6645.
32. Thompson MD, Monga SP. WNT/beta-catenin signaling in liver health and disease. HEPATOLOGY 2007;45:1298-1305.
33. Chen Y, Blackwell TW, Chen J, Gao J, Lee AW, States DJ. Integration of genome and chromatin structure with gene expression profiles to predict c-MYC recognition site binding and function. PLoS Comput Biol 2007;3:e63.
34. Alberts AS, Bouquin N, Johnston LH, Treisman R. Analysis of RhoA-binding proteins reveals an interaction domain conserved in heterotrimeric G protein beta subunits and the yeast response regulator protein Skn7. J Biol Chem 1998;273:8616-8622.
35. Peng J, Wallar BJ, Flanders A, Swiatek PJ, Alberts AS. Disruption of the Diaphanous-related formin Drf1 gene encoding mDia1 reveals a role for Drf3 as an effector for Cdc42. Curr Biol 2003;13:534-545.
36. Ariizumi S, Takasaki K, Yamamoto M, Ohtsubo T, Katsuragawa H, Katagiri S. Histopathologic differentiation of the main nodule determines outcome after hepatic resection for synchronous multicentric hepatocellular carcinomas. Hepatogastroenterology 2004;51:500-504.
37. Hu TH, Huang CC, Liu LF, Lin PR, Liu SY, Chang HW, et al. Expression of hepatoma-derived growth factor in hepatocellular carcinoma. Cancer 2003;98:1444-1456.
38. Kitamoto M, Nakanishi T, Kira S, Kawaguchi M, Nakashio R, Suemori S, et al. The assessment of proliferating cell nuclear antigen immunohistochemical staining in small hepatocellular carcinoma and its relationship to histologic characteristics and prognosis. Cancer 1993;72:1859-1865.
39. Hu L, Lau SH, Tzang CH, Wen JM, Wang W, Xie D, et al. Association of vimentin overexpression and hepatocellular carcinoma metastasis. Oncogene 2004;23:298-302.
40. Shah SA, Cleary SP, Wei AC, Yang I, Taylor BR, Hemming AW, et al. Recurrence after liver resection for hepatocellular carcinoma: risk factors, treatment, and outcomes. Surgery 2007;141:330-339.

# Common and specific roles of the related CDK inhibitors p27 and p57 revealed by a knock-in mouse model

Etsuo Susaki[a,b], Keiko Nakayama[b,c], Lili Yamasaki[d], and Keiichi I. Nakayama[a,b,1]

[a]Department of Molecular and Cellular Biology, Medical Institute of Bioregulation, Kyushu University, 3-1-1 Maidashi, Higashi-ku, Fukuoka, Fukuoka 812-8582, Japan; [b]CREST, Japan Science and Technology Agency, 4-1-8 Honcho, Kawaguchi, Saitama 332-0012, Japan; [c]Department of Developmental Biology, Center for Translational and Advanced Animal Research, Graduate School of Medicine, Tohoku University, 2-1 Seiryo, Aoba-ku, Sendai 980-8575, Japan; and [d]Department of Biological Sciences, Columbia University, New York, NY 10027

Edited by Charles J. Sherr, St. Jude Children's Research Hospital, Memphis, TN, and approved February 4, 2009 (received for review November 18, 2008)

**Although p27 and p57 are structurally related cyclin-dependent kinase inhibitors (CKIs), and are thought to perform similar functions, p27 knockout ($p27^{KO}$) and $p57^{KO}$ mice show distinct phenotypes. To elucidate the in vivo functions of these CKIs, we have now generated a knock-in mouse model ($p57^{p27KI}$), in which the p57 gene has been replaced with the p27 gene. The $p57^{p27KI}$ mice are viable and appear healthy, with most of the developmental defects characteristic of $p57^{KO}$ mice having been corrected by p27 knock-in. Such developmental defects of $p57^{KO}$ mice were also ameliorated in mice deficient in both p57 and the transcription factor E2F1, suggesting that loss of p57 promotes E2F1-dependent apoptosis. The developmental defects apparent in a few tissues of $p57^{KO}$ mice were unaffected or only partially corrected by knock-in expression of p27. Thus, these observations indicate that p57 and p27 share many characteristics in vivo, but that p57 also performs specific functions not amenable to substitution with p27.**

development | cell cycle | genetics

The regulation of cyclin-dependent kinase (CDK) activities is pivotal for the precisely ordered progression of the cell cycle. Such regulation is achieved by various mechanisms, including changes in the concentration, phosphorylation, and subcellular localization of cyclin–CDK complexes as well as in the interaction of CDKs with CDK inhibitors (CKIs) (1, 2). Two families of CKIs have been identified to date. The Cip-Kip family consists of p21 (Cip1), p27 (Kip1), and p57 (Kip2), and inhibits many types of cyclin-CDK complex, whereas the INK4 family includes p15, p16, p18, and p19, and specifically inhibits CDK4 or CDK6.

The CKIs p27 and p57 are structurally related proteins that share a conserved CDK binding-inhibitory domain and a QT domain in their $NH_2$- and COOH-terminal regions, respectively, and exhibit similar biochemical characteristics (3, 4). Also, several aspects of their cellular functions have suggested that these 2 CKIs are effectively "twin" molecules. For example, their expression levels are high in $G_0$ and $G_1$ phases of the cell cycle and decrease during progression from $G_1$ to S phase (5–10), in association with the activation of cyclin-CDK complexes. Such activation results in phosphorylation of Rb family proteins and consequent activation of transcription factors of the E2F family, which target genes required for entry into and progression through S phase. Consistent with this scenario, overexpression of either p27 or p57 in cultured cells induces $G_1$ arrest (3, 4, 6, 11).

Despite the similarities between p27 and p57, the phenotypes of p27 knockout ($p27^{KO}$) and $p57^{KO}$ mice differ substantially. Whereas $p27^{KO}$ mice are viable and show a hyperproliferative phenotype characterized by organ hyperplasia and tumorigenesis (12–14), consistent with the expected function of p27 as an inhibitor of cell proliferation, $p57^{KO}$ mice manifest neonatal death, as well as developmental defects in multiple tissues (15–17). These differences are possibly attributable to differences in the spatiotemporal patterns of p27 and p57 expression (18), to structural features of p57 not shared by p27 (Fig. 1*A*), or to differences in the interactions of the 2 CKIs with proteins other than CDKs (19–27). However, given that previous studies have not evaluated the intrinsic differences between p27 and p57 under physiological conditions, the differences in their in vivo roles have remained unclear.

To overcome such limitations of previous studies, and to compare directly the physiological roles of p27 and p57, we have now generated a knock-in mouse model in which the p57 gene has been replaced with the p27 gene, and in which p27 is, therefore, expressed instead of p57. Our genetic model has uncovered both common and unique features of p27 and p57 that manifest in a tissue-specific manner.

## Results

**Generation of $p57^{p27KI}$ Mice.** Both p27 and p57 possess a CKI domain in their $NH_2$-terminal regions and a QT domain that contributes to regulation of their stability at their COOH-termini, whereas mouse p57 contains a unique central domain that is not conserved in p27 or in human p57 (Fig. 1*A*). These structural characteristics led us to hypothesize that mouse p57 might have a specific role in development that is mediated through its central domain. Indeed, mouse p57 binds to LIM domain kinase (LIMK) through its central domain; thus, it regulates actin formation in chondrocytes (19). To investigate the functional equivalence and specificity of p27 and p57 in vivo, we developed a knock-in mouse model in which the endogenous p57 gene is replaced by a construct encoding hemagglutinin epitope (HA)-tagged mouse p27 (Fig. 1*B*). We showed that the HA tag did not impair the interaction of p27 with CDK2 or CDK4 in vivo (Fig. S1). Recombination events and removal of the *neo* cassette were confirmed by Southern blot analysis (Fig. 1*C*). The HA-p27 protein was expressed at the expected molecular size in embryonic tissues of, and in mouse embryonic fibroblasts (MEFs) derived from, the resulting $p57^{p27KI}$ mice (Fig. 1*D*; see also Fig. 4*A*). We confirmed that expression of HA-p27 under the control of the p57 gene promoter did not affect that of endogenous p27 (Fig. 1*D*). Also, the paternal knocked-in HA-p27 allele was not expressed in heterozygotes (Fig. 1*D*), suggesting that genomic imprinting, which normally suppresses expression of the paternal p57 allele, was not disturbed by the genetic manipulation. Thus, we crossed wild-type males and $p57^{+/-}$ or $p57^{+/p27KI}$ females, with the resulting

Author contributions: E.S., K.N., and K.I.N. designed research; E.S. performed research; L.Y. contributed new reagents/analytic tools; E.S. analyzed data; and E.S. and K.I.N. wrote the paper.

The authors declare no conflict of interest.

This article is a PNAS Direct Submission.

[1]To whom correspondence should be addressed. E-mail: nakayak1@bioreg.kyushu-u.ac.jp.

This article contains supporting information online at www.pnas.org/cgi/content/full/0811712106/DCSupplemental.

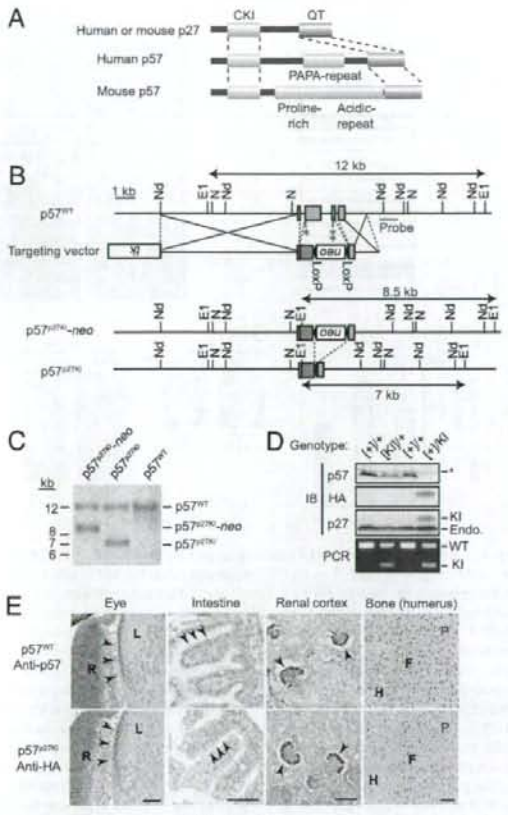


**Fig. 1.** Generation of $p57^{p27KI}$ mice. (*A*) Structures of p27 and p57. The 2 proteins share conserved CKI and QT domains in their $NH_2$- and COOH-terminal regions, respectively. Mouse p57 possesses a unique central domain that is not conserved in p27 or in human p57. (*B*) Schematic representations of the wild-type mouse p57 allele ($p57^{WT}$), the targeting vector, the knocked-in p27 allele with a LoxP-*neo* cassette ($p57^{p27KI}$-*neo*), and the knocked-in p27 allele after removal of the *neo* cassette by Cre recombinase. The expected sizes of DNA fragments that hybridize with the indicated probe in Southern blot analysis are shown. The ORF for mouse p27 tagged at its $NH_2$ terminus with HA is indicated by the red box. All introns of the p57 gene were removed in the resulting targeted allele to avoid splicing defects. E1, EcoRI; N, NotI; Nd, NdeI. Indicated are the initiation (1 asterisk) and stop (2 asterisks) codons of the p57 gene. (*C*) Southern blot analysis of EcoRI-digested DNA from ES cells harboring the indicated alleles. The sizes of the hybridizing fragments correspond to those indicated in *B*. (*D*) Immunoblot and PCR analyses of the expression and imprinting of the knocked-in p27 allele. Kidneys of newborn mice [postnatal day (P)0] were lysed and subjected to immunoblot analysis with antibodies to p57, to HA, and to p27. The asterisk indicates nonspecific bands, and the band positions for endogenous (Endo.) and knocked-in (KI) p27 are shown. Genomic DNA of the corresponding animals was subjected to PCR analysis to determine their genotypes. Brackets indicate a paternal imprinted allele. Both p57 and HA-p27 were expressed only from the maternal allele. WT and KI indicate the wild-type and knocked-in alleles, respectively. (*E*) Immunohistochemical analysis of the indicated tissues of wild-type ($p57^{WT}$) or $p57^{p27KI}$ neonates performed with antibodies to p57 or to HA. Sections were counterstained with hematoxylin. Arrowheads indicate the same types of cells expressing either p57 or HA-p27 in $p57^{WT}$ and $p57^{p27KI}$ mice, respectively. R, retina; L, lens; P, zone of proliferative cells; F, zone of flattened cells; H, zone of hypertrophic cells. (Scale bar, 50 $\mu$m.)

heterozygous offspring designated as $p57^{KO}$ or $p57^{p27KI}$ mice, respectively. Spatial expression patterns of HA-p27 in $p57^{p27KI}$ mice were almost identical to those of endogenous p57 in

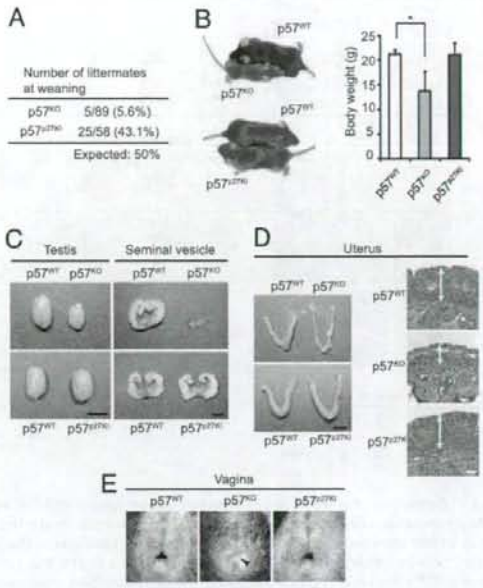


**Fig. 2.** Correction of adult $p57^{KO}$ mouse phenotypes in $p57^{p27KI}$ mice. (*A*) Number of littermates remaining at weaning from crosses between $p57^{WT}$ ($p57^{(+)/+}$) males and females harboring a paternal mutant allele ($p57^{(-)/+}$ or $p57^{(KI)/+}$). Thus, half of the littermates were expected to have a maternal mutant allele ($p57^{(+)/-}$ or $p57^{(+)/KI}$). (*B*) Representative animals and mean body weight for the indicated genotypes at 7 weeks of age. The animals of each pair shown are littermates. Quantitative data are means ± SD ($n$ = 3 to 7). *, $P < 0.05$ (ANOVA followed by Tukey–Kramer test). (*C* and *D*) Representative testes, seminal vesicles, and uteri from mice of each genotype at 7 weeks of age. Tissues of each pair were from littermates. Sections of the uterus were also subjected to hematoxylin-eosin staining; the muscle layer of the $p57^{KO}$ uterus was thinner than that of the $p57^{WT}$ or $p57^{p27KI}$ uteri (arrows). (Scale bars: macroscopic comparisons, 5 mm; uterine sections, 50 $\mu$m.) (*E*) Vaginal atresia (arrowhead) of a $p57^{KO}$ mouse at 7 weeks of age, and its correction in a $p57^{p27KI}$ mouse.

wild-type mice, with no substantial differences apparent in equatorial epithelial cells of the lens, gut epithelial cells, podocytes in the kidney, or cells of the proliferative to hypertrophic zones of epiphysial cartilage (Fig. 1*E*). Therefore, we concluded that the knocked-in HA-p27 allele was correctly expressed in place of the endogenous p57 allele with only a few exceptions apparent in some tissues (see below).

**Circumvention of Neonatal Death and Developmental Anomalies of $p57^{KO}$ Mice by Knock-In of p27.** Most $p57^{KO}$ mice die soon after birth, whereas some of them survive until weaning, but show marked growth retardation (Fig. 2 *A* and *B*; Table S1) (16). In contrast, $p57^{p27KI}$ mice were born in approximately the expected ratio, and grew at the same rate as wild-type littermates. Surviving $p57^{KO}$ mice manifest atrophy of various tissues or organs, including the seminal vesicle, testis, and uterus, as well as vaginal atresia (16), whereas such developmental anomalies were not apparent or were greatly ameliorated in $p57^{p27KI}$ mice (Fig. 2 *C–E*; Table S1). We further investigated whether specific defects apparent at birth in $p57^{KO}$ mice were corrected by the knock-in of p27. The growth retardation in utero, as well as developmental defects of the lens, palate, and intestine apparent with $p57^{KO}$ mice were absent or markedly diminished in $p57^{p27KI}$ mice (Fig. 3*A*; Table S1 and Fig. S2). Also, the enlargement of the adrenal gland apparent in $p57^{KO}$ mice was less pronounced

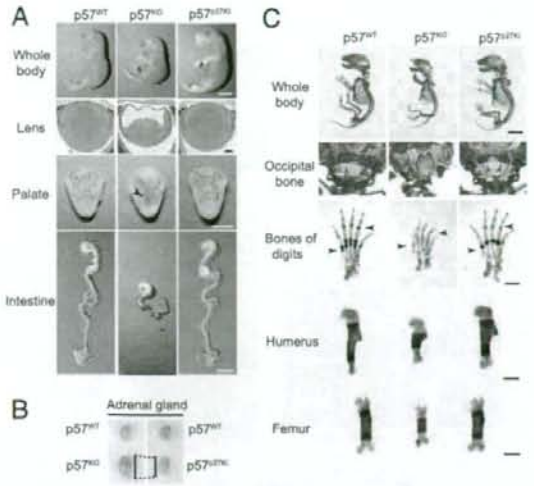


Fig. 3. Correction of embryonic p57$^{KO}$ mouse phenotypes in p57$^{p27KI}$ mice. (*A*) Representative examples of the whole body, lens, and palate at E18.5, as well as of the intestine at P0. The growth retardation, cataracts in the lens (stained with hematoxylin–eosin), cleft palate (arrowhead), and short intestine of p57$^{KO}$ mice were corrected in p57$^{p27KI}$ mice. (Scale bars: macroscopic comparisons, 5 mm; lens sections, 100 μm.) (*B*) Representative examples of the adrenal gland at P0. Vertical lines indicate comparison of the major axis between the glands from p57$^{KO}$ and p57$^{p27KI}$ mice. (*C*) Representative examples of skeletal staining of E18.5 embryos. Red and black arrowheads indicate the ossification of occipital bone and digits, respectively. (Scale bars: whole body, 5 mm; digits, humerus, and femur, 1 mm.)

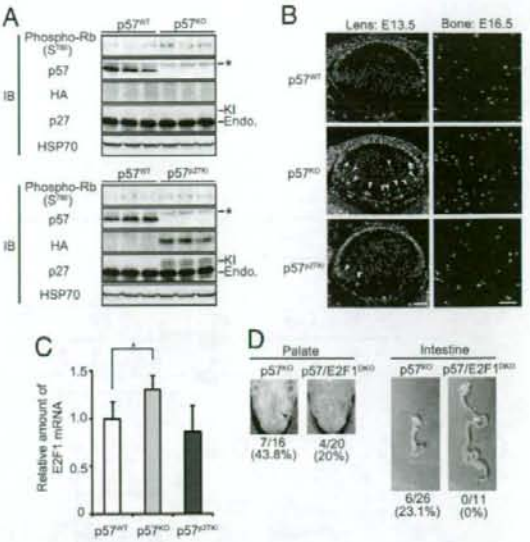


Fig. 4. Replacement of the CKI activity of p57 by knocked-in p27. (*A*) MEFs derived from p57$^{WT}$, p57$^{KO}$, or p57$^{p27KI}$ mice were deprived of serum (cultured in the presence of 1% FBS) for 48 h, lysed, and subjected to IP with antibodies to Rb followed by immunoblot analysis with antibodies to phosphorylated Rb (Ser$^{780}$). Lysates were also subjected directly to immunoblot analysis with antibodies to p57, to HA, to p27, and to HSP70 (loading control). Asterisk indicates nonspecific bands. The band positions for endogenous (Endo.) and knocked-in (KI) p27 are shown. Quantitative data for Rb phosphorylation are shown in Fig. S3*B*. (*B*) In situ BrdU incorporation was evaluated for embryos at E13.5 (lens) or E16.5 (zones of proliferative and flattened cells in the humerus). BrdU-positive cells, as well as nuclei stained with Hoechst 33258 (lens only) are green and gray, respectively. Arrowheads indicate ectopic BrdU-labeled cells in the posterior chamber of the lens. (Scale bar, 50 μm.) (*C*) Quantitative RT-PCR analysis of E2F1 expression in the intestine of E18.5 embryos. Normalized data for E2F1 mRNA are expressed relative to the corresponding value for wild-type mice, and are means ± SD ($n = 7$ or 8). *, $P < 0.05$ (ANOVA followed by Tukey–Kramer test). (*D*) Amelioration of cleft palate (arrowhead), and the intestinal defect of p57$^{KO}$ mice in p57/E2F1$^{DKO}$ mice. Penetrance of the defects at E17.5 (palate) and P0 (intestine) is indicated.

in p57$^{p27KI}$ mice (Fig. 3*B*; Table S1). The deformities of the vertebrae and ribs, delayed ossification of the occipital bone, digits, and long bones, and shortening of the long bones apparent in p57$^{KO}$ mice were also substantially corrected in p57$^{p27KI}$ mice (Fig. 3*C*; Table S1). These observations suggested that p27 is able to substitute for p57 in most tissues.

**Abnormal Inactivation of Rb in p57$^{KO}$ Mice Is Suppressed by Knock-In of p27.** Rb and related proteins have an important role in exit of cells from the cell cycle and in cell differentiation. The observation that p57$^{KO}$ mice show characteristics similar to those of mice deficient in Rb or Rb-related proteins, such as defects in lens and bone (28, 29), suggests that p57 regulates Rb-dependent pathways to ensure timely exit from the cell cycle and cell differentiation during development (2). To confirm that the knocked-in p27 in p57$^{p27KI}$ mice actually functions as a CKI, we prepared MEFs from wild-type, p57$^{KO}$, and p57$^{p27KI}$ mice, and evaluated endogenous cyclin-CDK activities. The extent of phosphorylation of Rb in serum-deprived p57$^{KO}$ MEFs was greater than that in wild-type MEFs (Fig. 4*A*; Fig. S3), although the difference was not pronounced, probably as a result of the higher level of expression of p27 than of p57 in MEFs, and the consequent limited impact of p57 loss. Knock-in of p27 significantly reduced the extent of Rb phosphorylation to a level similar to that apparent in the wild-type cells, suggesting that the ectopic p27 inhibited cyclin-CDK activities in place of p57 in arrested cells. To assess the CKI function of knocked-in p27 in vivo, we examined the extent of cell proliferation in lens and bone by measuring incorporation of BrdU at embryonic day (E)13.5 or E16.5, respectively. The numbers of BrdU-positive cells in lens (equatorial zone and posterior chamber) and bone (zones of proliferative and flattened cells) were increased in p57$^{KO}$ mice compared with those in wild-type mice, and these increases were largely abolished in p57$^{p27KI}$ mice (Fig. 4*B*). Thus, these results suggested that aberrant proliferation of cells in lens and bone of p57$^{KO}$ mice was inhibited by knock-in of p27, resulting in restoration of normal development of these tissues (Fig. 3 *A* and *C*).

Some developmental anomalies, such as the intestinal defect, of p57$^{KO}$ mice are likely attributable to aberrant apoptosis triggered by the lack of p57. Loss of p57 may result in inactivation of Rb by cyclin–CDK complexes and consequent induction of E2F1-dependent apoptosis, given that E2F1 contributes not only to proliferation but also, in some settings, to programmed cell death (30). We monitored E2F1 activity by determining the abundance of E2F1 mRNA, given that E2F1 activates transcription of its own gene in a positive feedback loop (31, 32). Indeed, the level of E2F1 mRNA was greater in the intestine of p57$^{KO}$ mice than in that of wild-type mice (Fig. 4*C*). In contrast, the amount of E2F1 mRNA in the intestine of p57$^{p27KI}$ mice was similar to that in wild-type animals. A role for E2F1-induced apoptosis in the developmental defects of p57$^{KO}$ mice was also confirmed by the substantial amelioration of the cleft palate and intestinal defect of p57$^{KO}$ mice that was apparent in p57/E2F1$^{DKO}$ mice (Fig. 4*D*), which were generated by crossing

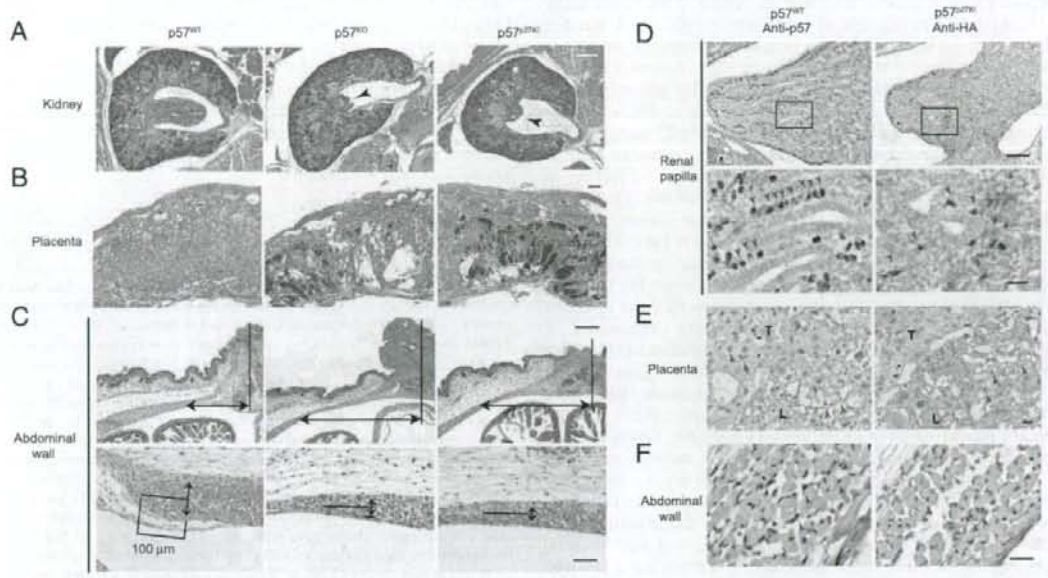


**Fig. 5.** Tissue-specific residual phenotypes and corresponding expression patterns of knocked-in p27 in $p57^{p27KI}$ mice. (*A* and *B*) Representative histopathology of the renal papilla and placenta, respectively, of E18.5 embryos of the indicated genotypes. Hematoxylin–eosin staining shows developmental defects in the renal papilla (arrowheads), and necrosis in the placenta of $p57^{KO}$ and $p57^{p27KI}$ mice. (Scale bar, 200 μm.) (*C*) Representative histopathology of the umbilical region (*Upper*), and the tip of the rectus abdominis muscle (*Lower*) of P0 embryos. Arrows indicate the distance between the umbilicus and the tip of the rectus abdominis muscle (U-M distance) (*Upper*), and the thickness of the muscle layer at a position 100 μm from the tip (*Lower*). Hematoxylin–eosin staining reveals an increased U-M distance and thinner muscle layer in both $p57^{KO}$ and $p57^{p27KI}$ mice. Quantitative data are shown in Fig. S4. (Scale bars: for *Upper*, 200 μm; for *Lower*, 50 μm.) (*D–F*) Immunohistochemical analysis of the renal papilla (E18.5), placenta (E18.5), and abdominal wall (P0), respectively, of $p57^{WT}$ or $p57^{p27KI}$ mice performed with antibodies to p57 or to HA, respectively. Sections were counterstained with hematoxylin. Arrowheads indicate corresponding cells expressing either p57 or knocked-in p27. The boxed regions in *D Upper* are shown at higher magnification in the *D Lower*. T, spongiotrophoblast zone; L, labyrinth zone. (Scale bars: for *D Upper*, 100 μm; for *D Lower*, *E*, and *F*, 20 μm.)

$p57^{KO}$ mice with $E2F1^{KO}$ mice (33). These observations suggest that p57 functions as a CKI in certain tissues during mouse development, and that it is replaceable in these tissues by p27.

**Phenotypes of $p57^{KO}$ Mice Not Corrected by Knock-In of p27.** Although most abnormalities of $p57^{KO}$ mice were found to be corrected in $p57^{p27KI}$ mice, there were some exceptions. Dysplasia of the renal papilla, placental dysplasia, and thinning of the abdominal wall or omphalocele, thus, remained in $p57^{p27KI}$ mice (Fig. 5 *A–C*; Table S1 and Fig. S4). These observations suggested that such phenotypes of the kidney, placenta, and abdominal wall are not responsible for the early death of $p57^{KO}$ mice. We examined the spatial expression patterns of p57 and HA-p27 in these tissues by immunohistochemical analysis. In the renal papilla of wild-type mice, p57 was found to be expressed predominantly in interstitial cells adjacent to renal tubular cells (Fig. 5*D*). Although the expression level of knocked-in p27 in $p57^{p27KI}$ mice appeared similar to that of p57 in wild-type mice, HA-p27 was detected in only a subset of interstitial cells, and the array of these cells was unorganized in $p57^{p27KI}$ mice (Fig. 5*D*). In the placenta, p57 was expressed both in trophoblasts of the basal and labyrinth zones, as well as in epithelial cells of the labyrinth zone in wild-type mice, whereas HA-p27 was virtually undetectable in trophoblasts of $p57^{p27KI}$ mice (Fig. 5*E*). Thus, persistent abnormalities observed in $p57^{p27KI}$ mice were associated with changes in the expression pattern of knocked-in p27, suggesting that regulation of the expression of p57 differs from that of HA-p27 in a cell type-dependent manner. RT-PCR analysis revealed that the expression of HA-p27 mRNA in the kidney or placenta of $p57^{p27KI}$ mice was similar to that of endogenous p57 mRNA in wild-type mice (Fig. S5*A*). Also, immunohistofluorescence analysis showed that KPC (34) and Pirh2 (35; T. Hattori and M. Kitagawa, personal communication), both of which are p27-specific E3 ubiquitin ligases, were expressed prominently in the trophoblast layer, but to a lesser extent in the labyrinth layer of the placenta (Fig. S5*B*), suggesting that HA-p27, but not p57, may undergo ubiquitin-dependent degradation in trophoblasts. In contrast, the expression pattern of HA-p27 in epithelial cells of the labyrinth zone, as well as in skeletal muscle cells of the abdominal wall appeared similar to that of p57 (Fig. 5 *E* and *F*), despite the remaining mutant phenotypes in $p57^{p27KI}$ mice (Fig. 5 *B* and *C*), suggesting that p57 has a specific role in these tissues. Together, these various observations suggest that p57 and p27 share many roles in vivo, but that p57 also performs specific functions not amenable to substitution with p27.

## Discussion

We have examined whether the in vivo functions of p27 and p57 are identical by generating a knock-in mouse model in which the p57 gene is replaced with the p27 gene. The $p57^{p27KI}$ mice were born in the expected numbers and survived without gross abnormalities, whereas most $p57^{KO}$ mice manifest multiple developmental defects, and die shortly after birth. The inactivation of the Rb pathway and increased cell proliferation, as well as the associated developmental defects that result from p57 deficiency, were corrected by knock-in of p27. Thus, our data

show, in a physiological setting, that p27 and p57 are functionally similar, with p27 being able to substitute for p57, and that the CKI activity, rather than other potential functions, of p57 is critical for development of most tissues. Our observations support the notion that differences between the phenotypes of $p27^{KO}$ and $p57^{KO}$ mice are mainly attributable to differences in the spatial and temporal expression patterns of p27 and p57 (18), as well as to differences in the sensitivities of tissues to insufficient inhibition of cell proliferation, rather than to differences in the intrinsic molecular activities of the 2 proteins. The abundance of p27 is greater than that of p57 in some tissues, whereas that of p57 is greater than that of p27 in others (18). Thus, the former tissues may be less sensitive than the latter to the ablation of p57. For example, the amount of p27 is greater than that of p57 in MEFs, consistent with the observation that the ablation of p57 in these cells results in only a moderate change in CKI activity (this study), and a minimal biological effect (16).

In humans, the p57 gene maps to chromosomal region 11p15.5, which is implicated in Beckwith–Wiedemann syndrome (BWS) (36, 37). BWS is characterized by various growth abnormalities, some of which are recapitulated in $p57^{KO}$ mice (17, 38, 39). Given that the central domains of human and mouse p57 differ, the well-conserved CKI domain may be responsible for the abnormalities shared by $p57^{KO}$ mice and BWS patients. Knock-in of p27 corrected many of these abnormalities, including cleft palate, enlargement of the adrenal gland, as well as intestinal, skeletal, and lens defects, supporting the idea that the conserved CKI domain has a key role in organ development not only in mice but also in humans.

The defects in some tissues of $p57^{KO}$ mice remained apparent in $p57^{p27KI}$ mice. Also, slight defects sometimes remained even in tissues that showed recovery. These findings might be explained by several possible scenarios. First, there might be differences in the activity or specificity of p27 and p57 as CKIs. Indeed, phosphorylation of p27 at tyrosine residues 74, 88, and 89 affects its binding preferences and CKI activity (40–43). Thus, it is possible that cell type-specific kinases phosphorylate CKIs and, thus, regulate their CDK-inhibitory activity. Second, non-CKI functions of p27 and p57 may be important for developmental processes. Both p27 and p57 bind various molecules specifically (20–27, 44), and contribute to certain developmental processes in a manner independent of their CKI activity (22, 25, 45–48). For example, stabilization of MyoD and inhibition of JNK by p57 promote myoblast differentiation (23, 26, 49), consistent with our finding that knocked-in p27 did not correct the abdominal muscle defect of $p57^{KO}$ mice, despite its expression pattern being apparently identical to that of p57. Also, given that mouse p57 binds to LIMK through its unique central domain to regulate actin formation (19), and that LIMK2 knockout mice manifest abnormalities in the kidney (50), defective cell migration might be responsible for the kidney defect of $p57^{KO}$ mice. Third, the stability of p27 and p57 proteins may also differ in a cell type-dependent manner. The expression level of knocked-in p27 in placental trophoblasts of $p57^{p27KI}$ mice was greatly reduced compared with that of p57 in wild-type mice, suggesting the existence of a posttranscriptional regulatory mechanism specific for p27 in these cells. Indeed, there appear to be specific pathways for p27 or p57 degradation. Only p27 (not p57) is ubiquitylated by the KPC-dependent pathway (34), or by Pirh2-dependent pathway (35; T. Hattori and M. Kitagawa, personal communication), whereas the F-box protein FBL12 was recently shown to contribute to the degradation of p57 (51). Thus, various mechanisms may determine the specific features of p27 and p57.

In conclusion, p27 and p57 possess similar CKI activities, but each of the 2 proteins shows specific features in certain cellular contexts. The extent of correction of the developmental defects of $p57^{KO}$ mice by p27 knock-in varied in a tissue-dependent manner, presumably reflecting the extent to which p27 and p57 are molecularly equivalent.

## Materials and Methods

For more details, see *SI Materials and Methods*.

**Generation of $p57^{p27KI}$ Mice.** The knock-in mouse was generated as described previously (14, 16). The targeting vector was constructed by replacement of exons 2 and 3, which contain the ORF, as well as intron 2 of the p57 gene with a cDNA encoding HA-tagged mouse p27 as well as with a neomycin-resistance gene (*neo*) cassette flanked by LoxP sequences. The 5′ region of homology in the targeting vector consisted of a 1.6-kb fragment generated by PCR with appropriate primers to remove intron 3 of the p57 gene; the 3′ region of homology comprised a 7-kb fragment generated by PCR with appropriate primers to remove intron 1, and connected an NdeI-NotI fragment spanning the promoter region and 5′ untranslated region of the p57 gene. The ES cell clones that manifested homologous recombination were subjected to an additional electroporation to introduce the Cre-Pac vector (52), and puromycin-resistant, G418-sensitive colonies were isolated. Examination of embryonic and neonatal phenotypes was performed with mice of the C57BL/6J background or the C57BL/6J × 129/Sv background, whereas adult phenotypes were examined on the C57BL/6J × 129/Sv background, because most $p57^{KO}$ mice die at birth on the C57BL/6J background.

**Immunoprecipitation (IP) and Immunoblot Analysis (IB).** Kidneys of newborn mice or E13.5 MEFs were lysed in radioimmunoprecipitation assay (RIPA) buffer supplemented with phosphatase and protease inhibitor (PPI) mix (10 mM sodium pyrophosphate/10 mM NaF/2 mM sodium orthovanadate/1 mM phenylmethylsulfonyl fluoride/10 μg/mL aprotinin/20 μg/mL leupeptin). MEF lysates were subjected to IP with antibodies to Rb (BD PharMingen) in IP buffer (0.5% Triton X-100/150 mM NaCl/PPI mix). Primary antibodies for IB included those to p57 (P-0357, Sigma), to HA (HA-11, Covance), to p27 (BD TDL), to Rb phosphorylated on $Ser^{780}$ (Cell Signaling), and to HSP70 (BD TDL).

**Histology, Immunostaining, and Skeletal Staining.** Hematoxylin–eosin staining was performed according to the standard protocol. Immunohistochemical analysis was performed as described previously (18), with the use of antibodies to p57 (H-91, Santa Cruz Biotechnology) or to HA (Y-11, Santa Cruz Biotechnology). E18.5 embryos were subjected to skeletal staining as described previously (16).

**BrdU Incorporation.** Embryos were labeled for 2 h with BrdU by i.p. injection of dams (100 μg of BrdU per gram of body weight). Paraffin-embedded tissue was sectioned at a thickness of 3 μm (lens, E13.5) or 4 μm (humerus, E16.5), and was immunostained with biotinylated antibodies to BrdU (BD PharMingen) and Alexa 488-conjugated streptavidin (Molecular Probes). Nuclei were stained with Hoechst 33258.

**Quantitative RT-PCR Analysis.** Total RNA was extracted and purified from the intestine of E18.5 embryos and subjected to reverse transcription with a QuantiTect kit (Qiagen). The resulting cDNA was subjected to real-time PCR analysis as described previously (53), with 200 nM primers specific for E2F1 (54) or GAPDH (53). The abundance of E2F1 mRNA was normalized relative to that of GAPDH mRNA.

**ACKNOWLEDGMENTS.** We thank M. Kitagawa for discussion; N. Kitajima, Y. Yamada, and K. Takeda for technical assistance; members of our laboratories for comments on the manuscript; and A. Ohta and M. Kimura for help in preparation of the manuscript. This work was supported in part by a grant from the Ministry of Education, Science, Sports, and Culture of Japan, and by a research grant from the Takeda Science Foundation.

1. Sherr CJ, Roberts JM (1999) CDK inhibitors: Positive and negative regulators of G1-phase progression. *Genes Dev* 13:1501–1512.
2. Nakayama KI, Nakayama K (1998) Cip/Kip cyclin-dependent kinase inhibitors: Brakes of the cell cycle engine during development. *BioEssays* 20:1020–1029.
3. Lee M-H, Reynisdottir I, Massague J (1995) Cloning of $p57^{KIP2}$, a cydin-dependent kinase inhibitor with unique domain structure and tissue distribution. *Genes Dev* 9:639–649.
4. Matsuoka S, et al. (1995) $p57^{KIP2}$, a structurally distinct member of the $p21^{CIP1}$ Cdk inhibitor family, is a candidate tumor suppressor gene. *Genes Dev* 9:650–662.
5. Polyak K, et al. (1994) $p27^{Kip1}$, a cyclin-Cdk inhibitor, links transforming growth factor-β and contact inhibition to cell cycle arrest. *Genes Dev* 8:9–22.
6. Toyoshima H, Hunter T (1994) p27, a novel inhibitor of G1 cyclin-Cdk protein kinase activity, is related to p21. *Cell* 78:67–74.

7. Hengst L, Dulic V, Slingerland JM, Lees E, Reed SI (1994) A cell cycle-regulated inhibitor of cyclin-dependent kinases. *Proc Natl Acad Sci USA* 91:5291–5295.
8. Nourse J, et al. (1994) Interleukin-2 mediated elimination of the p27(Kip1) cyclin-dependent kinase inhibitor prevented by rapamycin. *Nature* 372:570–573.
9. Reynisdottir I, Polyak K, Iavarone A, Massague J (1995) Kip/Cip and Ink4 Cdk inhibitors cooperate to induce cell cycle arrest in response to TGF-β. *Genes Dev* 9:1831–1845.
10. Kamura T, et al. (2003) Degradation of $p57^{Kip2}$ mediated by $SCF^{Skp2}$-dependent ubiquitylation. *Proc Natl Acad Sci USA* 100:10231–10236.
11. Polyak K, et al. (1994) Cloning of $p27^{Kip1}$, a cyclin-dependent kinase inhibitor and a potential mediator of extracellular antimitogenic signals. *Cell* 78:59–66.
12. Fero ML, et al. (1996) A syndrome of multiorgan hyperplasia with features of gigantism, tumorigenesis, and female sterility in $p27^{Kip1}$-deficient mice. *Cell* 85:733–744.
13. Kiyokawa H, et al. (1996) Enhanced growth of mice lacking the cyclin-dependent kinase inhibitor function of $p27^{Kip1}$. *Cell* 85:721–732.
14. Nakayama K, et al. (1996) Mice lacking $p27^{Kip1}$ display increased body size, multiple organ hyperplasia, retinal dysplasia, and pituitary tumors. *Cell* 85:707–720.
15. Yan Y, Frisen J, Lee M-H, Massague J, Barbacid M (1997) Ablation of the CDK inhibitor $p57^{Kip2}$ results in increased apoptosis and delayed differentiation during mouse development. *Genes Dev* 11:973–983.
16. Takahashi K, Nakayama KI, Nakayama K (2000) Mice lacking a CDK inhibitor, $p57^{Kip2}$, exhibit skeletal abnormalities and growth retardation. *J Biochem* 127:73–83.
17. Zhang P, et al. (1997) Altered cell differentiation and proliferation in mice lacking $p57^{KIP2}$ indicates a role in Beckwith-Wiedemann syndrome. *Nature* 387:151–158.
18. Nagahama H, et al. (2001) Spatial and temporal expression patterns of the cyclin-dependent kinase (CDK) inhibitors $p27^{Kip1}$ and $p57^{Kip2}$ during mouse development. *Anat Embryol* 203:77–87.
19. Yokoo T, et al. (2003) $p57^{Kip2}$ regulates actin dynamics by binding and translocating LIM-kinase 1 to the nucleus. *J Biol Chem* 278:52919–52923.
20. Laman H, et al. (2005) Transforming activity of Fbxo7 is mediated specifically through regulation of cyclin D/cdk6. *EMBO J* 24:3104–3116.
21. Besson A, Gurian-West M, Schmidt A, Hall A, Roberts JM (2004) $p27^{Kip1}$ modulates cell migration through the regulation of RhoA activation. *Genes Dev* 18:862–876.
22. Nguyen L, et al. (2006) $p27^{kip1}$ independently promotes neuronal differentiation and migration in the cerebral cortex. *Genes Dev* 20:1511–1524.
23. Chang T-S, et al. (2003) $p57^{KIP2}$ modulates stress-activated signaling by inhibiting c-Jun $NH_2$-terminal kinase/stress-activated protein kinase. *J Biol Chem* 278:48092–48098.
24. Joaquin M, Watson RJ (2003) The cell cycle-regulated B-Myb transcription factor overcomes cyclin-dependent kinase inhibitory activity of $p57^{KIP2}$ by interacting with its cyclin-binding domain. *J Biol Chem* 278:44255–44264.
25. Joseph B, et al. (2003) $p57^{Kip2}$ cooperates with Nurr1 in developing dopamine cells. *Proc Natl Acad Sci USA* 100:15619–15624.
26. Reynaud EG, et al. (2000) Stabilization of MyoD by direct binding to $p57^{Kip2}$. *J Biol Chem* 275:18767–18776.
27. Watanabe H, et al. (1998) Suppression of cell transformation by the cyclin-dependent kinase inhibitor $p57^{KIP2}$ requires binding to proliferating cell nuclear antigen. *Proc Natl Acad Sci USA* 95:1392–1397.
28. Morgenbesser SD, Williams BO, Jacks T, DePinho RA (1994) p53-dependent apoptosis produced by Rb-deficiency in the developing mouse lens. *Nature* 371:72–74.
29. Cobrinik D, et al. (1996) Shared role of the pRB-related p130 and p107 proteins in limb development. *Genes Dev* 10:1633–1644.
30. Putzer BM (2007) E2F1 death pathways as targets for cancer therapy. *J Cell Mol Med* 11:239–251.
31. Hsiao KM, McMahon SL, Farnham PJ (1994) Multiple DNA elements are required for the growth regulation of the mouse E2F1 promoter. *Genes Dev* 8:1526–1537.
32. Neuman E, Flemington EK, Sellers WR, Kaelin WG, Jr (1994) Transcription of the E2F-1 gene is rendered cell cycle dependent by E2F DNA-binding sites within its promoter. *Mol Cell Biol* 14:6607–6615.
33. Degregori J, Leone G, Miron A, Jakoi L, Nevins JR (1997) Distinct roles for E2F proteins in cell growth control and apoptosis. *Proc Natl Acad Sci USA* 94:7245–7250.
34. Kamura T, et al. (2004) Cytoplasmic ubiquitin ligase KPC regulates proteolysis of $p27^{Kip1}$ at G1 phase. *Nat Cell Biol* 6:1229–1235.
35. Hattori T, et al. (2007) Pirh2 promotes ubiquitin-dependent degradation of the cyclin-dependent kinase inhibitor $p27^{Kip1}$. *Cancer Res* 67:10789–10795.
36. Koufos A, et al. (1989) Familial Wiedemann-Beckwith syndrome and a second Wilms tumor locus both map to 11p15.5. *Am J Hum Genet* 44:711–719.
37. Ping AJ, et al. (1989) Genetic linkage of Beckwith-Wiedemann syndrome to 11p15. *Am J Hum Genet* 44:720–723.
38. Swanger WJ, Roberts JM (1997) $p57^{KIP2}$ targeted disruption and Beckwith-Wiedemann syndrome: Is the inhibitor just a contributor? *BioEssays* 19:839–842.
39. Caspary T, et al. (1999) Oppositely imprinted genes $p57^{Kip2}$ and Igf2 interact in a mouse model for Beckwith-Wiedemann syndrome. *Genes Dev* 13:3115–3124.
40. Kardinal C, et al. (2006) Tyrosine phosphorylation modulates binding preference to cyclin-dependent kinases and subcellular localization of $p27^{Kip1}$ in the acute promyelocytic leukemia cell line NB4. *Blood* 107:1133–1140.
41. Grimmler M, et al. (2007) Cdk-inhibitory activity and stability of $p27^{Kip1}$ are directly regulated by oncogenic tyrosine kinases. *Cell* 128:269–280.
42. Chu I, et al. (2007) p27 phosphorylation by src regulates inhibition of cyclin E-Cdk2. *Cell* 128:281–294.
43. James MK, Ray A, Leznova D, Blain SW (2008) Differential modification of $p27^{Kip1}$ controls its cyclin D-cdk4 inhibitory activity. *Mol Cell Biol* 28:498–510.
44. Nakanishi M, Kaneko Y, Matsushime H, Ikeda K (1999) Direct interaction of p21 cyclin-dependent kinase inhibitor with the retinoblastoma tumor suppressor protein. *Biochem Biophys Res Commun* 263:35–40.
45. Messina G, et al. (2005) $p27^{Kip1}$ acts downstream of N-cadherin-mediated cell adhesion to promote myogenesis beyond cell cycle regulation. *Mol Biol Cell* 16:1469–1480.
46. Kawauchi T, Chihama K, Nabeshima Y-I, Hoshino M (2006) Cdk5 phosphorylates and stabilizes $p27^{Kip1}$ contributing to actin organization and cortical neuronal migration. *Nat Cell Biol* 8:17–26.
47. Dugas JC, Ibrahim A, Barres BA (2007) A crucial role for $p57^{Kip2}$ in the intracellular timer that controls oligodendrocyte differentiation. *J Neurosci* 27:6185–6196.
48. Dyer MA, Cepko CL (2000) $P57^{Kip2}$ regulates progenitor cell proliferation and amacrine interneuron development in the mouse retina. *Development* 127:3593–3605.
49. Reynaud EG, Pelpel K, Guillier M, Leibovitch MP, Leibovitch SA (1999) $p57^{Kip2}$ stabilizes the MyoD protein by inhibiting cyclin E-Cdk2 kinase activity in growing myoblasts. *Mol Cell Biol* 19:7621–7629.
50. Takahashi H, Koshimizu U, Miyazaki J-I, Nakamura T (2002) Impaired spermatogenic ability of testicular germ cells in mice deficient in the LIM-kinase 2 gene. *Dev Biol* 241:259–272.
51. Kim M, Nakamoto T, Nishimori S, Tanaka K, Chiba T (2008) A new ubiquitin ligase involved in $p57^{KIP2}$ proteolysis regulates osteoblast cell differentiation. *EMBO Rep* 9:878–884.
52. Taniguchi M, et al. (1998) Efficient production of Cre-mediated site-directed recombinants through the utilization of the puromycin resistance gene, pac: A transient gene-integration marker for ES cells. *Nucleic Acids Res* 26:679–680.
53. Onoyama I, et al. (2007) Conditional inactivation of Fbxw7 impairs cell-cycle exit during T cell differentiation and results in lymphomatogenesis. *J Exp Med* 204:2875–2888.
54. David G, et al. (2008) Specific requirement of the chromatin modifier mSin3B in cell cycle exit and cellular differentiation. *Proc Natl Acad Sci USA* 105:4168–4172.

nature
cell biology

# CHD8 suppresses p53-mediated apoptosis through histone H1 recruitment during early embryogenesis

Masaaki Nishiyama[1,2], Kiyotaka Oshikawa[1,2], Yu-ichi Tsukada[1,2], Tadashi Nakagawa[1,2], Shun-ichiro Iemura[3], Tohru Natsume[3], Yuhong Fan[4,5], Akira Kikuchi[6], Arthur I. Skoultchi[4] and Keiichi I. Nakayama[1,2,7]

**The chromodomain helicase DNA-binding (CHD) family of enzymes is thought to regulate gene expression, but their role in the regulation of specific genes has been unclear. Here we show that CHD8 is expressed at a high level during early embryogenesis and prevents apoptosis mediated by the tumour suppressor protein p53. CHD8 was found to bind to p53 and to suppress its transactivation activity. CHD8 promoted the association of p53 and histone H1, forming a trimeric complex on chromatin that was required for inhibition of p53-dependent transactivation and apoptosis. Depletion of CHD8 or histone H1 resulted in p53 activation and apoptosis. Furthermore, *Chd8*$^{-/-}$ mice died early during embryogenesis, manifesting widespread apoptosis, whereas deletion of *p53* ameliorated this developmental arrest. These observations reveal a mode of p53 regulation mediated by CHD8, which may set a threshold for induction of apoptosis during early embryogenesis by counteracting p53 function through recruitment of histone H1.**

Although apoptosis has a key role in organization of the developing embryo, it is not fully understood how apoptosis is regulated during embryogenesis. The tumour suppressor protein p53 mediates the induction of apoptosis in response to DNA damage caused by genotoxic stress. It activates the transcription of numerous genes, and thereby triggers cell-cycle arrest, senescence or apoptosis to prevent tumorigenesis[1–5].

Activation of transcription by p53 is regulated, at least in part, by the amount of p53 as well as by post-translational modifications of p53 (refs 6–8). In addition, certain chromatin-associated proteins that change chromatin configuration interact with p53 and thereby modulate its transactivation activity[5,8–12]. Although these findings suggest that chromatin configuration may affect the transactivation activity of p53, the mechanism by which the structure of chromatin changes, as well as the biological outcome of such regulation, have remained largely unknown.

Certain classes of molecules recognize modified histones and are thought to translate the modification code into specific functions. Such proteins include members of the chromodomain helicase DNA-binding (CHD) family of enzymes, which also belong to the SNF2 superfamily of ATP-dependent chromatin remodellers[13–15]. Chd1 of *Saccharomyces cerevisiae* is a component of the multi-subunit histone acetyltransferase complexes SAGA and SLIK[16], and is required for methylation of histone H3 at Lys 4 (H3K4; ref. 17). Human CHD1 catalyses the ATP-dependent transfer of histones from the NAP-1 chaperone to DNA, resulting in the assembly of active chromatin[18,19]. Nine genes for CHD1-related proteins have been identified in mammalian species.

Among these proteins, CHD8 (Duplin) was originally isolated as a negative regulator of the Wnt–β-catenin signalling pathway[20]. The carboxy-terminal region of CHD8 interacts with the insulator-binding protein CTCF, and this interaction is important for insulator activity[21]. We previously generated *Chd8*$^{-/-}$ mice and showed that these animals die *in utero* between embryonic day (E) 5.5 and E7.5, manifesting widespread apoptosis[22]. However, Wnt activation was not seen in the *Chd8*$^{-/-}$ embryos before their death. Although these observations suggest that CHD8 may possess anti-apoptotic activity that is independent of Wnt signalling inhibition, it has been unclear how the loss of CHD8 induces apoptosis. We now show that CHD8 binds to both p53 and histone H1, and that these interactions facilitate recruitment of histone H1 to p53 target genes, resulting in suppression of their expression and of apoptosis induced by genotoxic insults. These results thus suggest that loss of CHD8 in mice induces apoptosis as a result of unrestrained p53 activity at the early stage of embryonic development. Consistent with this conclusion, deletion of *p53* in *Chd8*$^{-/-}$ mice ameliorated the developmental arrest. The physiological role of CHD8 may thus be to prevent such unwanted apoptosis during early embryogenesis.

[1]Department of Molecular and Cellular Biology, Medical Institute of Bioregulation, Kyushu University, 3-1-1 Maidashi, Higashi-ku, Fukuoka, Fukuoka 812-8582, Japan. [2]CREST, Japan Science and Technology Agency (JST), Kawaguchi, Saitama 332-0012, Japan. [3]National Institute of Advanced Industrial Science and Technology (AIST), Biological Information Research Center (JBIRC), Kohtoh-ku, Tokyo 135-0064, Japan. [4]Department of Cell Biology, Albert Einstein College of Medicine, 1300 Morris Park Avenue, Bronx, NY 10461, USA. [5]School of Biology and the Petit Institute for Bioengineering and Bioscience, Georgia Institute of Technology, IBB 2313, 315 Ferst Drive, Atlanta, GA 30332-0363, USA. [6]Department of Biochemistry, Graduate School of Biomedical Sciences, Hiroshima University, 1-2-3 Kasumi, Minami-ku, Hiroshima 734-8551, Japan.
[7]Correspondence should be addressed to K.I.N. (e-mail: nakayak1@bioreg.kyushu-u.ac.jp)

Received 29 July 2008; accepted 28 October 2008; published online 18 January 2009; DOI: 10.1038/ncb1831

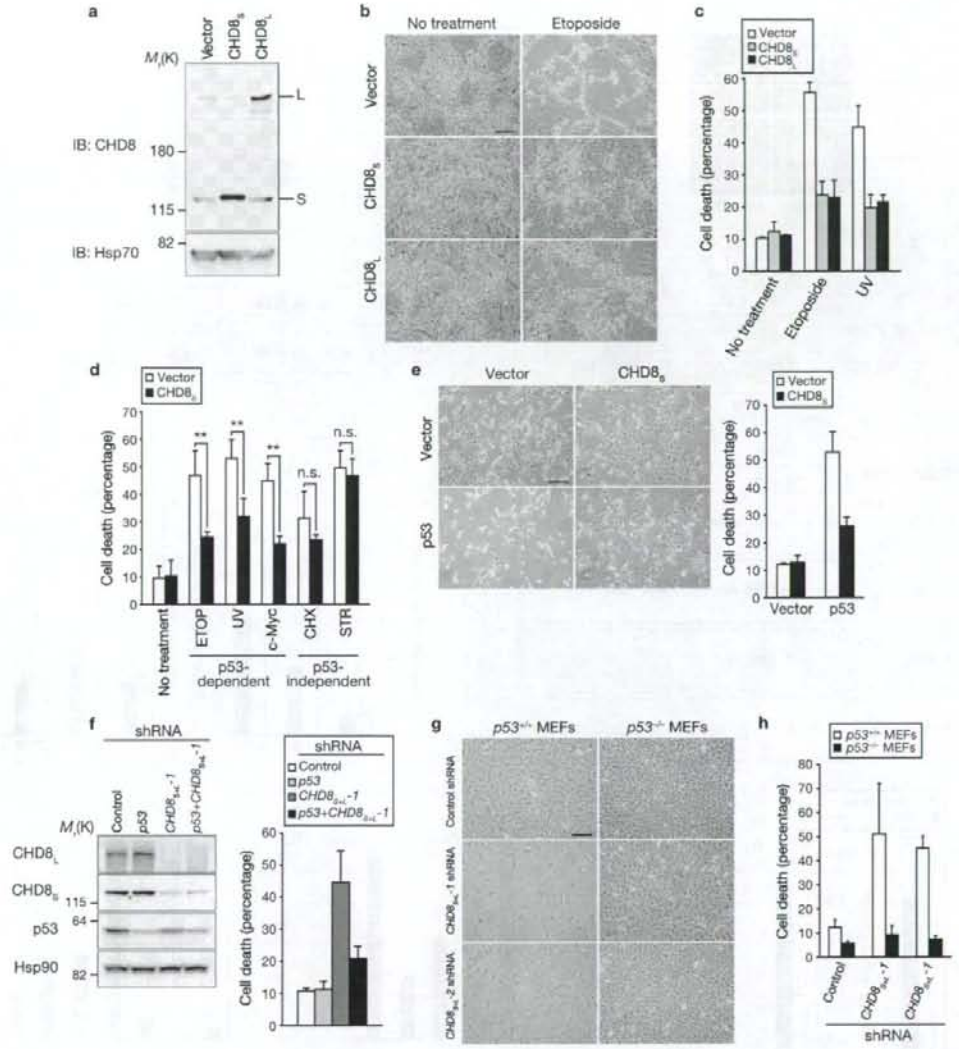


**Figure 1** Anti-apoptotic activity of CHD8. (**a–c**) NIH 3T3 cells overexpressing $CHD8_S$ or $CHD8_L$ were subjected to immunoblot (IB, **a**) analysis with anti-CHD8 and exposed to genotoxic stress. Cells were examined by phase-contrast microscopy (**b**) and the percentage of dead cells was determined by trypan blue staining (**c**). Data in **c** are mean ± s.d., $n = 3$. (**d**) NIH 3T3 cells overexpressing $CHD8_S$ were exposed to etoposide (ETOP, 50 μM), cycloheximide (CHX, 100 μg ml$^{-1}$), staurosporine (STR, 1 μM), UV radiation or c-Myc overexpression. Data in **d** are mean ± s.d., $n = 3$ (**$P < 0.01$; n.s., not significant; $P > 0.05$; Student's *t*-test). (**e**) U2OS cells were infected with retroviral vectors for $CHD8_S$ or p53 and were stained with trypan blue (left panel). Data shown in the right panel are mean ± s.d., $n = 3$. (**f**) U2OS cells were infected with retroviral vectors encoding shRNAs specific for *p53*, both $CHD8_S$ and $CHD8_L$ (*$CHD8_{S+L}$-1*) or *EGFP* (control), subjected to immunoblotting (left panel), stained with trypan blue and the percentage of dead cells determined (right panel). Data shown in the right panel are mean ± s.d., $n = 3$. (**g**, **h**) $p53^{+/+}$ or $p53^{-/-}$ MEFs infected with retroviral vectors for *$CHD8_{S+L}$-1* or *$CHD8_{S+L}$-2* shRNAs were examined by phase-contrast microscopy (**g**) and the percentage of dead cells determined by trypan blue staining (**h**). Data in **h** are mean ± s.d., $n = 3$. Scale bars are 100 μm (**b**, **e**, **g**).

## RESULTS

### CHD8 suppresses p53-dependent apoptosis

Mouse *Chd8* consists of 37 exons spanning about 40 kb. Alternative splicing of exon 9 generates two transcripts that encode a protein ($CHD8_L$) with a relative molecular mass of 280,000 ($M_r$ 280K), containing two chromodomains (a helicase/ATPase domain and a DNA binding domain) and a 110K protein ($CHD8_S$, also known as Duplin), which contains only the amino-terminal chromodomain (Supplementary Information, Fig. S1a, b). These molecules are expressed in most cell lines and tissues (Supplementary Information, Fig. S1c, d), but the ratio of $CHD8_L$ to $CHD8_S$ varies.